Clim Dyn
DOI 10.1007/s00382-014-2184-7

Reconstructing the subsurface ocean decadal variability using surface nudging in a perfect model framework

Jérôme Servonnat · Juliette Mignot · Eric Guilyardi · Didier Swingedouw · Roland Séférian · Sonia Labetoulle

Received: 19 June 2013 / Accepted: 16 May 2014

Abstract Initialising the ocean internal variability for decadal predictability studies is a new area of research and a variety of *ad hoc* methods are currently proposed. In this study, we explore how nudging with sea surface temperature (SST) and salinity (SSS) can reconstruct the three-dimensional variability of the ocean in a perfect model framework. This approach builds on the hypothesis that oceanic processes themselves will transport the surface information into the ocean interior as seen in ocean-only simulations. Five nudged simulations are designed to reconstruct a 150 years "target" simulation, defined as a portion of a long control simulation. The nudged simulations differ by the variables restored to, SST or SST + SSS, and by the area where the nudging is applied. The strength of the heat flux feedback is diagnosed from observations and the restoring coefficients for SSS use the same time-scale. We observed that this choice prevents spurious convection at high latitudes and near sea-ice border when nudging both SST and SSS. In the tropics, nudging the SST is enough to reconstruct the tropical atmosphere circulation and the associated dynamical and thermodynamical impacts on the underlying ocean. In the tropical Pacific Ocean, the profiles for temperature show a significant correlation from the surface down to 2,000 m, due to dynamical adjustment of the isopycnals. At mid-to-high latitudes, SSS nudging is required to reconstruct both the temperature and the salinity below the seasonal thermocline. This is particularly true in the North Atlantic where adding SSS nudging enables to reconstruct the deep convection regions of the target. By initiating a previously documented 20-year cycle of the model, the SST + SSS nudging is also able to reproduce most of the AMOC variations, a key source of decadal predictability. Reconstruction at depth does not significantly improve with amount of time spent nudging and the efficiency of the surface nudging rather depends on the period/events considered. The joint SST + SSS nudging applied everywhere is the most efficient approach. It ensures that the right water masses are formed at the right surface density, the subsequent circulation, subduction and deep convection further transporting them at depth. The results of this study underline the potential key role of SSS for decadal predictability and further make the case for sustained large-scale observations of this field.

Keywords Initialisation · Nudging · Decadal climate predictability · Ocean dynamics · Atlantic meridional overturning circulation · Salinity

J. Servonnat (✉) · J. Mignot · E. Guilyardi · S. Labetoulle
LOCEAN/IPSL, Paris, France
e-mail: Jerome.Servonnat@lsce.ipsl.fr

J. Servonnat · D. Swingedouw · R. Séférian
LSCE/IPSL, Gif-sur-Yvette, France

J. Servonnat · J. Mignot · E. Guilyardi · D. Swingedouw · R. Séférian · S. Labetoulle
CNRM-GAME, Toulouse, France

J. Mignot
Climate and Environmental Physics, Physics Institute, Oeschger Centre of Climate Change Research, University of Bern, Bern, Switzerland

E. Guilyardi
NCAS-Climate, University of Reading, Reading, UK

1 Introduction

Decadal predictability is an emerging research challenge in the climate science community. Studies have suggested

Published online: 13 June 2014

that some features of the climate system are potentially predictable at decadal to multidecadal time scales (Collins and Sinha 2003; Hawkins and Sutton 2009; Keenlyside et al. 2008; Msadek et al. 2010; Persechino et al. 2013; Swingedouw et al. 2013), notably in the ocean. This potential predictability relies partly on forced variability like anthropogenic or volcanic forcing, but also, in some regions, on internal variability (Cox and Stephenson 2007; Hawkins and Sutton 2009).

While coupled climate models are only able to capture some aspects of internal variability of the climate in a statistical sense, a given historical simulation driven solely by external forcing of the twentieth century has no a priori reason to reproduce the observed internal decadal variability in terms of phase and amplitude. In this context and similarly to weather and seasonal forecasts, initialisation procedures are used to bring the model to a trajectory as close as possible to the observed climate. Because of the time scales and inertia involved, predictability at decadal timescales first requires initialising the ocean. Most of current approaches initialise the ocean alone but initialisation with coupled assimilation procedures are emerging (e.g. Zhang et al. 2007) and the initialisation of other "slow" components is also considered (sea-ice, land, stratosphere).

Modelling groups have been exploring various techniques and methodologies for the initialisation, as described in Meehl et al. (in press). The current approaches can be distinguished by the depth of the ocean initialization procedure (surface or at depth) and whether anomalies or full fields are used. One method is to restore (or "nudge") the model surface variables (e.g. SST) to their observed counterparts, as done in Keenlyside et al. (2008) or Swingedouw et al. (2013). Other methods use nudging to subsurface temperature and salinity datasets (Pohlmann et al. 2009; Smith et al. 2007) or ocean data assimilation schemes (Stepanov et al. 2012; Zhang et al. 2007). Zhang et al. (2010) compared the performance of different data sets in the ocean in reconstructing variations of he AMOC. Their findings show that surface nudging may initialize variations of the AMOC, but incorporating subsurface data clearly improves performances. Because of model biases, full-field initialisation methods drive the model away from its own mean state, and usually lead to an important initial drift during the forecast; removing this drift is a delicate issue that involves a number of *ad hoc* hypotheses. Anomaly initialisation, in which the observation anomalies are added to the model mean state, partly overcomes this problem. However, some issues remain, especially in regions where the model's variability patterns do not match that of observations (e.g. western boundary currents). Another strategy is to apply directly a reanalysed oceanic state as starting conditions for the coupled hindcasts (Du et al. 2012; Kröger et al. 2012). In this case, there is no initialized simulation, only initial conditions, but this also leads to a strong "initial shock" of the forecast due to coupled model biases.

This diversity of approaches to reconstruct an initial state is due to a combination of factors: the lack of quality multi-decadal three-dimensional ocean observations, the presence of climate model errors and drift, the impact of external forcing, the large range of space and time scales involved, to name the main ones. As a consequence, defining the most effective initialisation strategy is a challenge and none has yet been identified as "the best". It is therefore key to better understand how the different initialisation techniques operate in a climate model.

To that effect and to overcome some of the limitations listed above, this question can be explored in a perfect model framework (e.g. Dunstone and Smith 2010). The experimental set up is as follows. A sequence is first extracted from a control model simulation (using constant external forcing) and is defined as the "target", i.e. a surrogate observation dataset. The goal is then to restore the model to a subset of variables of this target, and then assess if the reconstructed simulation follows the target trajectory for different variables and phenomena. Working in a perfect unforced model framework allows focusing on internal variability (i.e. the goal of initialisation), to overcome the data limitation and model biases issues, and to provide robust statistics. The limitations are that comparison with observations is not possible and that the understanding gained in this simple framework does not necessarily translate into real cases application and initialisation because, for example, of external forcing (that can play a role in initialising oceanic processes, as shown in Swingedouw et al. (2013) for volcanic eruptions in the IPSL-CM5A-LR coupled model), model biases, or uncertainty in the observations. We nevertheless take the view that understanding the processes involved in the initialisation of the models is a prerequisite to using the models to understand the real world.

We here decide to try to reconstruct the ocean state by surface nudging only given the greater availability and quality of surface versus interior data. To gain as much physical understanding as possible on how the restoring operates on the ocean, we choose to work in a perfect model framework. The goal is to drive the model towards the observed trajectory while keeping coherent internal dynamics, which is a major source of predictability. Ocean interior nudging or initialisation might be potentially detrimental to internal dynamics (issues associated with the model biases found both at the surface and at depth). This surface nudging strategy assumes that oceanic processes themselves will transport the surface information into the ocean interior through relevant processes (e.g. subduction

or convection). This is the strategy retained for the contribution of the Institute Pierre Simon Laplace (IPSL) to the near term simulations of CMIP5 that focused on the last 50 years (Taylor et al. 2012). Swingedouw et al. (2013) have shown that this strategy gives encouraging results in terms of Atlantic Meridional Overturning Circulation (AMOC) initialisation and 2-m temperature around the North Atlantic sector. Other studies using other initialisation approaches do not yield radically different results, one reason being that the external forcing, such as volcanoes, is a major source of predictability (Kim et al. 2012; Doblas-Reyes et al. 2013).

Up to now surface restoring has mostly involved SST. This restoring is applied using a Haney (1971) relaxation term, $\gamma_T\left(SST_{model} - SST_{target}\right)$, as was done to force ocean-only simulations before the more physically based bulk formulas were introduced [such as in ocean-only CORE simulations (Griffies et al. 2009)]. The relaxation term γ_T can be diagnosed from observations by measuring oceanic heat flux feedback (e.g. Barnier et al. 1995, Frankignoul and Kestenare 2002) and is estimated to be about -40 W/m^2/K. Most of previous initialisation studies used a much larger relaxation coefficient γ_T (60 times larger in Luo et al. (2005), 15 times in Keenlyside et al. (2008) and Dunstone and Smith (2010), 6 times in Pohlmann et al. (2009)). The benefit of a very large γ_T is that the SST is constrained to remain very close to observations. The downside is that when the SST is not mostly driven by surface fluxes (e.g. strongly advective regions) the mismatch between the model of the observations drives unphysical high restoring heat fluxes (that can reach 1000 s of W/m^2), creating subsurface water masses with wrong properties and jeopardising the ocean interior, a key source of predictability. Sea surface salinity (SSS) is usually not used to initialise coupled models for at decadal predictability. One reason is that SSS is poorly observed at decadal time scales. However, salinity is a key property of the ocean, affecting its density, water mass formation, deep convection, etc. (e.g. Laurian et al. (2006); Swingedouw et al. (2007a), Mignot and Frankignoul (2009)) and it is of prime interest to see how initialising the ocean with SSS nudging can improve the reconstruction of the subsurface ocean in the ocean model.

In this study, we explore how SST and SSS surface nudging using physically based restoring coefficients can reconstruct the three-dimensional structure of the ocean in a perfect model framework. The assessment of the influence of the associated initialisation on the predictability using hindcasts (e.g. Persechino et al. 2013) is an important question but it is beyond the scope of the present study. The paper is organised as follows. Section 2 presents the experimental setup including the description of the climate model used (IPSL-CM5A-LR), and the nudged simulations performed. Section 3 presents the SST and SSS response to the nudging in the different simulations and Sects. 4 and 5 concentrates on the temperature and salinity response at depth in the tropics and at mid-to-high latitudes, respectively. Section 6 explores the AMOC reconstruction using the different nudging strategies. Section 7 provides a summary and a discussion of the paper's results.

2 Experimental setup and method

2.1 Climate model

The CMIP5 version of the Institut Pierre Simon Laplace coupled model, IPSL-CM5A-LR, described in details in Dufresne et al. (2013), is used. The atmospheric model is LMDZ5A (Hourdin et al. 2013), with a resolution of 96 × 96 × L39. It is associated with the ORCHIDEE land surface model (Krinner et al. 2005) and coupled to the Nucleus of a European Modelling of the Ocean (NEMO) framework (Madec 2008) with the coupler OASIS3 (Valcke 2012). NEMO is composed of OPA9.0 for the ocean and LIM2 for the sea ice (Fichefet and Maqueda 1997), both implemented on an ORCA2.0 tripolar grid. The horizontal resolution is 2° on average, refined to 0.5° in the tropics, with 31 vertical levels. NEMO also integrates the PISCES biogeochemistry module (Aumont and Bopp 2006). IPSL-CM5A-LR has been used in particular in studies on decadal variability (Escudier et al. 2013) and on decadal predictability (Persechino et al. 2013; Swingedouw et al. 2013).

2.2 Nudged simulations set up

This work is based on the stable 1,000-year long pre-industrial control simulation provided for CMIP5, available on the ESGF distributed database (e.g. http://esgf-node.ipsl.fr). The simulated climate is in equilibrium, as described in Dufresne et al. (2013). We consider a 150-year sequence of this simulation as a target dataset (instead of using observations). This period was selected in the control run as it includes several high amplitude peaks in the AMOC index, as defined by the maximum of the annual mean of the Atlantic meridional overturning circulation between 20 and 60°N below 500 m (Fig. 1, see also Persechino et al. 2013).

An independent time period is also selected as the "original" simulation (thick black curve in Fig. 1), which initial state is used for the nudged simulations. These simulations are nudged towards the surface ocean variables (SST or SSS) of the target. We consider both a restoring to

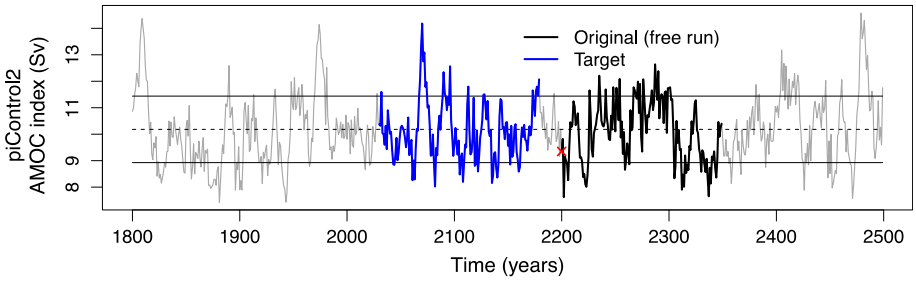

Fig. 1 Target (*blue*) and free run (*black*) periods shown in the AMOC time series from the 1,000-year long preindustrial control simulation (*grey*). The *red cross* shows the restart for all the nudged simulations. The *dashed horizontal line* highlights the mean, and the *two horizontal black solid lines* highlight plus or minus one standard deviation of the long term (1,000 years) AMOC index

SST only and to SST + SSS in different sensitivity simulations. As described in the introduction, the nudging is done via a Haney restoring term, which acts as an additional heat (freshwater) flux added to the equations of heat (salt) conservations:

$$\frac{\partial SST}{\partial t} = \ldots + \frac{\gamma_T}{\rho C_P h}\left(SST_{model} - SST_{target}\right); \gamma_T = -40\,\mathrm{W/m^2/K} \quad (1)$$

$$\frac{\partial SSS}{\partial t} = \ldots + \frac{\gamma_S}{h}\left(SSS_{model} - SSS_{target}\right); \gamma_S = -864\,\mathrm{mm/day} \quad (2)$$

$\frac{\partial SST}{\partial t}$ and $\frac{\partial SSS}{\partial t}$ are the time derivative of surface temperature and salinity, SST_{model} and SSS_{model} are the instantaneous SST and SSS in the running model, and SST_{target} and SSS_{target} are the SST and SSS in the target at the corresponding time step; γ_T and γ_S are the restoring coefficients that control the strength of the nudging and h is the depth of the considered surface layer. The coefficient γ_T is taken equal to the physically based value of -40 W/m^2/K (Frankignoul and Kestenare 2002) which corresponds to a relaxation timescale of about 60 days for a 50 m deep mixed layer. Unlike γ_T which mimics the observed temperature/heat fluxes relationship, SSS relaxation has no physical basis and we choose the value of γ_S so that the typical relaxation time scale is similar to that of SST i.e. -864 mm/day which also corresponds to a relaxation timescale of about 60 days for a 50 m deep mixed layer. Such a choice ensures consistency in terms of restoring strength (timescale) between SST and SSS restoring.

SST nudging alone in the sea-ice edge region can create spurious buoyancy forcing: for a given grid point, if sea ice is present in the target but not in the running nudged simulation the term ($SST_{model} - SST_{target}$) can easily reach several degrees. This leads to negative heat fluxes reaching hundreds of W/m^2, anomalously dense waters and spurious oceanic convection (Dunstone and Smith 2010). Keenlyside et al. (2008) overcame the problem by limiting the nudging area equatorward of 60°N. Yet, given the importance of high latitudes for the large-scale ocean circulation and decadal variability, such limitation is an issue. We describe below the solutions we investigated.

Table 1 Summary of the setups for the nudged simulations (left column); Second column indicates the area where the restoring is applied (illustrated on Fig. 2); third and last column indicates if a restoring to SST and to SSS (respectively) is applied

Initialisation experiment	Restoring area	Restoring to SST	Restoring to SSS
SST_40 deg	Equatorward of 40°	Yes	No
SST_Full	Globe	Yes	No
SST_NoSic	No restoring if SST < 0 in the target or the nudged experiment	Yes	No
SST + SSS_Full	Globe	Yes	Yes
SST + SSS_NoSic	No restoring if SST < 0 in the target or the nudged experiment	Yes	Yes

We ran a set of five different nudged simulations with the same target, starting from the same initial conditions and using different nudging strategies. The setup of the simulations is summarized in Table 1 and Fig. 2. The first three simulations, SST_Full, SST_NoSic and SST_40 deg, are restored to SST only while the last two, SST + SSS_Full and SST + SSS_NoSic, are restored to SST and SSS. The suffix of the simulation name denotes the area where the nudging is applied (Fig. 2).

In SST_Full and SST_40 deg, the restoring area is fixed: in SST_Full all ocean and sea ice grid points are nudged; in SST_40 deg, only the points equatorward of 40° are nudged. Compared to Keenlyside et al. (2008), we restricted the restoring area abruptly to 40° (and not with a transition region between 30° and 60°) because IPSL-CM5A-LR can have sea-ice south of 60°N in winter under preindustrial conditions. In SST_NoSic, the nudging only occurs when the SST is positive, a simple and conservative estimation of the time-varying sea-ice free ocean. Nudging

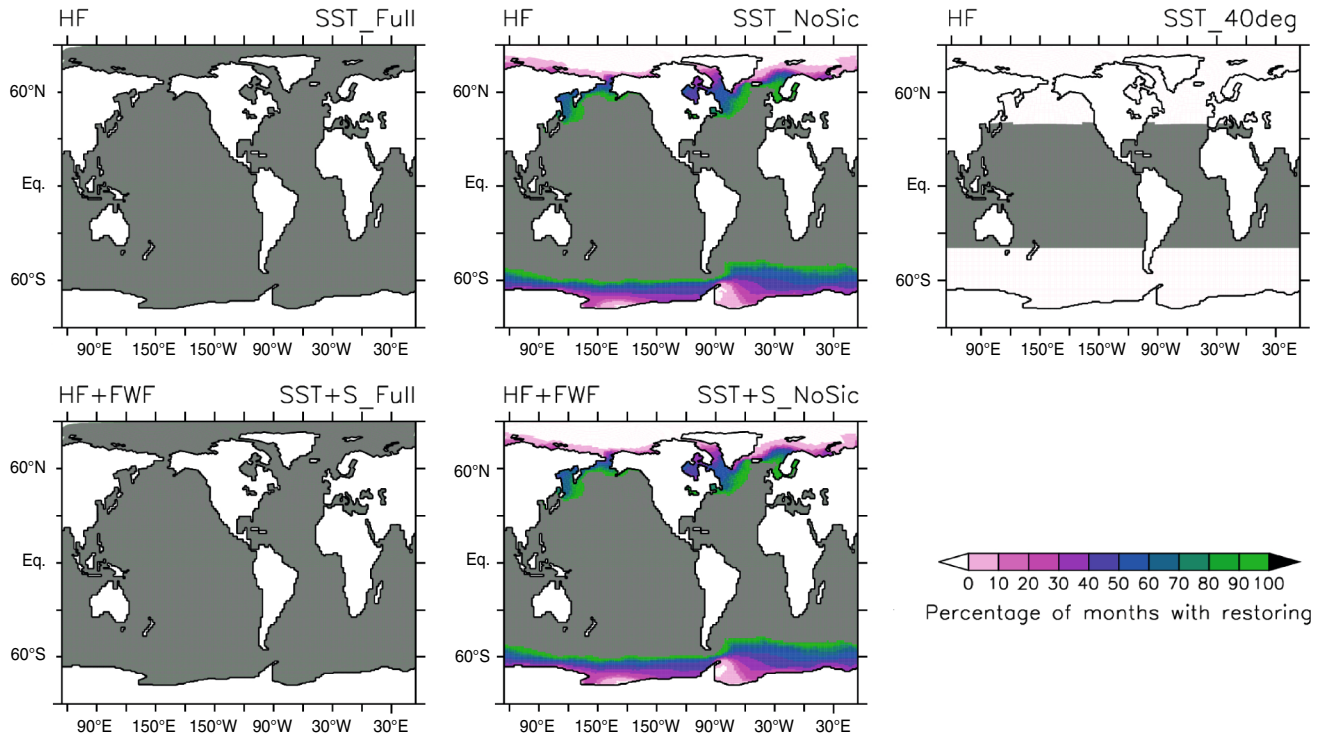

Fig. 2 Percentage of months when restoring was effectively applied with respect to the total lengths for each nudged experiment identified in the *upper right* of each panel. In the *upper left* of the panels is indicated whether the simulation consists in SST restoring only (HF) or both SST and SSS restoring (HF + FWF). The *white* and the *grey* shadings highlight the area with no restoring at all and always restoring on the whole period, respectively. The other *colours* show that the restoring is not done systematically, i.e. there is a condition on whether to restore or not

occurrence is expressed in percentage of months when restoring was effectively applied with respect to of the total period length for each nudged experiment in Fig. 2. SST_NoSic is very similar to the initialisation adopted for the IPSL CMIP5 short-term predictability simulations (Swingedouw et al. 2013). Note that for all simulations, there is no buffer region between nudged and free regions. The two additional simulations SST + SSS_Full and SST + SSS_NoSic have the same nudging areas as SST_Full and SST_NoSic respectively, but the nudging is also applied to SSS (Table 1). All simulations cover the whole 150 years of the target.

Note here that the NoSic runs essentially differ from the Full runs in the subpolar regions, and were designed for issues related to the AMOC. We will see that they are very similar to the Full runs outside the sea-ice covered latitudes. In those regions they can be considered as supplementary members that strengthen the findings with SST_Full and SST + SSS_Full.

In order to evaluate the effect of the surface nudging, we compare the nudged simulations both with the target and the original (unperturbed) trajectory of the model, referred to as the free run (thin black line in Fig. 1). The goal is to quantify if, where, and after which adjustment period, a simulation is closer to the target than the free simulation. We use correlations (significance estimated with Student *t* tests) to estimate how the variability of two simulations is phased in time, and Fisher F test to estimate if the variance ratio of two simulations is different from one (i.e. if the variance of an experiment is not equal to the variance of the target; Von Storch and Zwiers (2002), see appendix for the details of the statistical methods used; whether this is the variance of the nudged simulation that is significantly higher than the variance of the target, or the contrary, will be mentioned in the text describing the results).

3 Surface reconstruction using SST and SSS nudging

In this section the effect of the nudging on surface variables, including the SST and SSS themselves, is assessed. The analysis is done using annual means and over the 150 years since most of the surface response is obtained after 2 months (timescale of the restoring coefficient for a mixed layer of 50 m). Note that these results are unchanged after removing the first ten to thirty years of the simulations (not shown), suggesting little interannual adjustment in the surface initialisation. The same analysis was also done

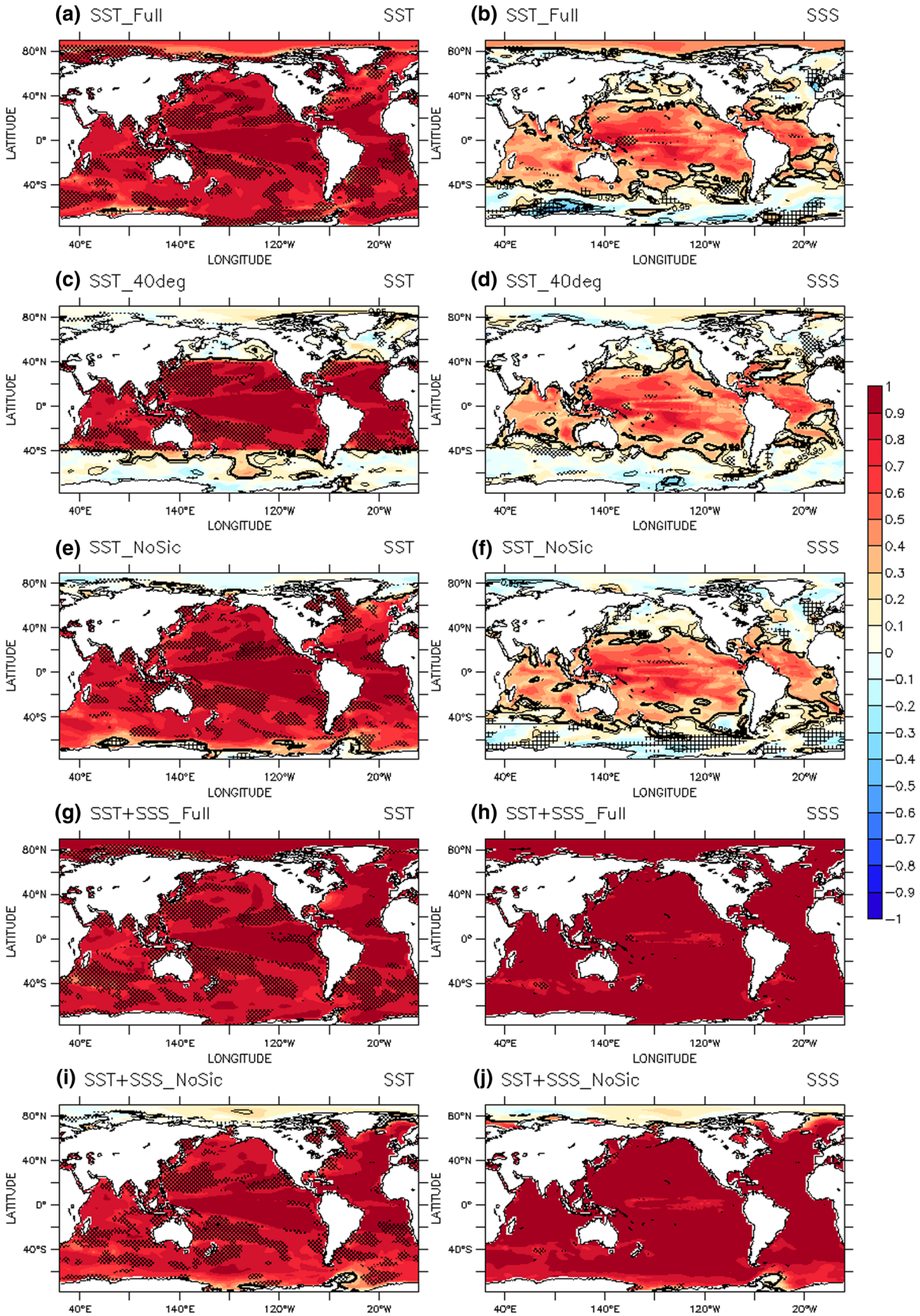
(a) SST_Full SST
(b) SST_Full SSS
(c) SST_40deg SST
(d) SST_40deg SSS
(e) SST_NoSic SST
(f) SST_NoSic SSS
(g) SST+SSS_Full SST
(h) SST+SSS_Full SSS
(i) SST+SSS_NoSic SST
(j) SST+SSS_NoSic SSS
LATITUDE
LONGITUDE
80°N
40°N
0°
40°S
40°E
140°E
120°W
20°W
1
0.9
0.8
0.7
0.6
0.5
0.4
0.3
0.2
0.1
0
−0.1
−0.2
−0.3
−0.4
−0.5
−0.6
−0.7
−0.8
−0.9
−1

◀**Fig. 3** Correlation coefficient estimated between the target and the different nudged simulations: SST_Full (**a**, **b**), SST_40 deg (**c**, **d**), SST_NoSic (**e**, **f**), SST + SSS_Full (**g**, **h**) and SST + SSS_NoSic (**i**, **j**), for the SST (**a**, **d**, **e**, **g** and **i**) and SSS (**b**, **d**, **f**, **h** and **j**). The correlation coefficients are calculated on yearly time series. The *thin* and *thick contours underline* the 95 and 99 % level of the Student *t* test for the correlation. The *shaded areas* highlight where the Fisher *F* test are significant at more than 99 %; the hatching shows where the standard deviation ratio (nudged/target) is greater than one, and the point pattern shows where the standard deviation ratio is lower than one

using seasonal means or 11-year filtered time series (not shown) and showed similar features, with a slight increase in correlation for the 11-year filtering (potentially linked with the auto-correlation of the series).

3.1 Sea surface temperature

Figure 3 (left panels) shows maps of SST correlation between the nudged simulations and the target. The correlation patterns of the different nudged simulations follow the area where the nudging is applied. In SST_40 deg (Fig. 3c), significant correlation coefficients are also found outside the nudging area, mainly in the South Pacific and, to a lower extent, in the North Atlantic. For all simulations, the correlation coefficients are above 0.8 (statistically significant at the 99 % level) almost everywhere in the restoring area, indicating that the nudging, even with a "low" coefficient, has led to a correct initialisation of the SST where it is applied.

Within the area of significant correlations (99 % level), we can see that some oceanic regions show higher values than others. One explanation to this correlation pattern is the relative influence of processes acting on timescales faster than, or of the order of, 2 months (i.e. the relaxation timescale) on SST variability. These processes include advection (western boundary currents, Antarctic circumpolar current), convection (Greenland-Island-Norwegian Seas) or heat fluxes. Another reason is that the mixed layer is deeper than the 50 m assumption (mainly in extra-tropical latitudes and during winter) used to define the restoring coefficient and the nudging term is not strong enough to fully control the evolution of the mixed-layer temperature, hence that of the SST.

The comparison of the simulations with SST + SSS nudging and the simulations with SST nudging only shows that restoring to SSS further improves the SST reconstruction (higher correlation) at mid to high latitudes, particularly in the North Atlantic, the Arctic and the Southern Ocean.

Significant differences in variance between the nudged simulations and the target mainly occur the mid-latitudes (40–20°S and 20–40°N, shaded areas in Fig. 3) in the Pacific, South Atlantic and Indian oceans. They cover a somewhat wider area in SST_40 deg, SST + SSS_Full and SST + SSS_NoSic. For these regions, the Fisher F test shows significantly lower variability in the nudged simulations than in the target. The standard deviation ratio is generally larger than 0.7 but can reach 0.6 locally (not shown). In these regions, the typical ocean mixed layer time scale is near the two-month relaxation time scale used for the nudging. The SST restoring is therefore damping the heat fluxes driven variations. In the tropics, in contrast, the latent heat flux and the surface currents are constrained via the SST driven atmosphere circulation (see below) and contribute to the higher correlation coefficients and a ratio of variance close to one. The results are similar when considering a root mean squared error computation between target and nudged simulations (not shown).

3.2 Sea surface salinity and hydrological budget

For the simulations with restoring to SST only (Fig. 3, panels b, d, and f) the SSS correlation coefficients are significant at the 99 % level in the tropical band (30°S–30°N) only, with values between 0.5 and 0.8. Moreover, apart from the Pacific warm pool in SST_Full (lower variability), the F test is not rejected in the tropics. This contrasted behaviour further suggests that heat fluxes due to SST-atmosphere interactions are indeed responsible for the reduced variance in SST at mid-latitudes, as discussed above.

Nudging the SST is able to reconstruct the evaporation minus precipitation (E-P hereafter) hydrological budget in the Tropics (Fig. 4d), especially within the 10°S/10°N latitudinal band. This is associated with the reconstruction of the SST forced Tropical interannual atmospheric variability, as shown in Fig. 4: the 10 m-wind (Fig. 4a, b) and the vertical velocity at 500mb (Fig. 4c) in SST_Full are significantly correlated to the target between 20°S and 20°N. The correlation pattern follows the regions of high variability that are commonly linked with the Walker circulation: along the equator for the westward zonal 10-m wind, on both sides (divergence) of the equator for the meridional 10-m wind and the horseshoe pattern on the Western Pacific for the vertical velocity at 500mb. This reconstruction of the deep tropical atmospheric circulation is able to drive the reconstruction of the E-P budget near the equator. SSS is mostly driven by E-P in the tropics (Yu 2011; Zhang et al. 2012; Zheng and Zhang 2012) and this explains why the SSS correlation is higher in the tropics than in the rest of the globe when only SST is nudged. Comparing Figs. 4d and 3f further shows that the reconstructed SSS area in the tropical area has a 10° wider meridional extension than the reconstructed E-P budget, especially along the western oceanic boundaries. This is attributed to the poleward advection of the E-P driven reconstructed SSS by the mean currents (arrows on Fig. 4d).

In the SST + SSS experiments, the correlation coefficients for SSS (Fig. 3, panels h and j) are between 0.9 and

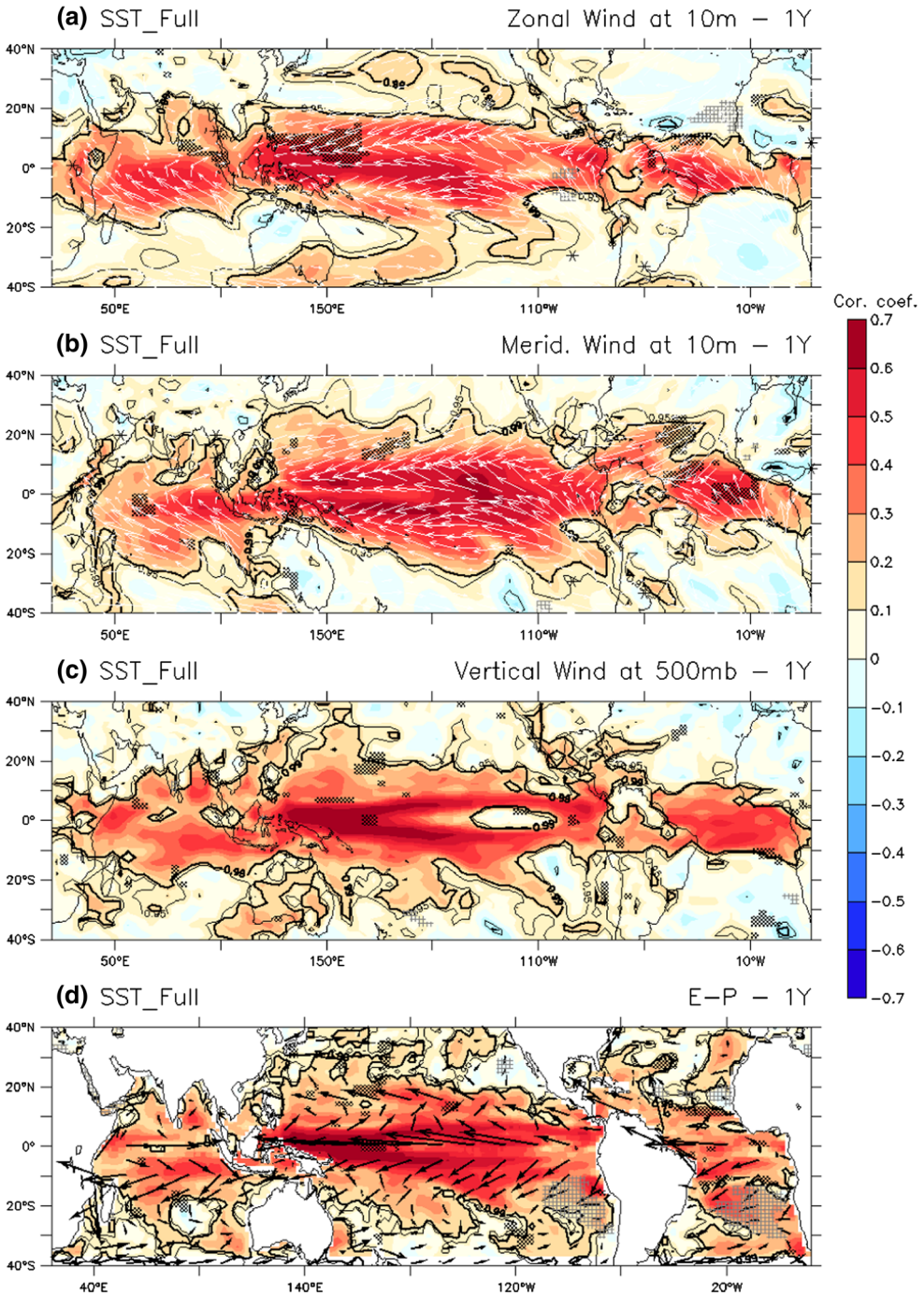

Fig. 4 Correlation between the target and SST_Full for the 10 m-wind zonal (**a**) and meridional (**b**) components, the vertical velocity at 500 mb (**c**) and the E–P budget (**d**). The *thick* and *thin contour lines* underline the coefficients significant at the 99 and 95 % level respectively. The *white arrows* on panels **a** and **b** (no unit) show the climatological 10 m-wind. The *black arrows* on panel **d** show the surface ocean currents (no unit). The *shaded areas* highlight where the Fisher *F* test are significant at more than 99 %; the hatching highlight where the standard deviation ratio (nudged/target) is greater than one and the point pattern where it is lower than one

1 almost everywhere there is nudging, although it drops to 0.7 in some regions. This result shows the efficiency of the restoring term on SSS. This is due to the absence of an atmospheric feedback on SSS anomalies—unlike SST and heat fluxes—thereby increasing its persistence (e.g. Mignot and Frankignoul 2003). Consequently the processes controlling SSS variability tend to act on longer timescales than the processes controlling SST variability, which explain that, with the same relaxation time scale, SSS nudging is more efficient than SST nudging. The minima on the correlation pattern on Fig. 3h and j however suggest that processes acting on time scales faster than the 2-month restoring time scale (as for SST) tend to slightly modulate the SSS nudging efficiency (with correlation coefficients still above 0.8 within those minima). Indeed, the regions with lower correlation correspond to regions with larger high frequency variance for SSS and SST (not shown).

In the simulations with SST nudging only, the F test shows a significantly (99 % confidence) higher SSS

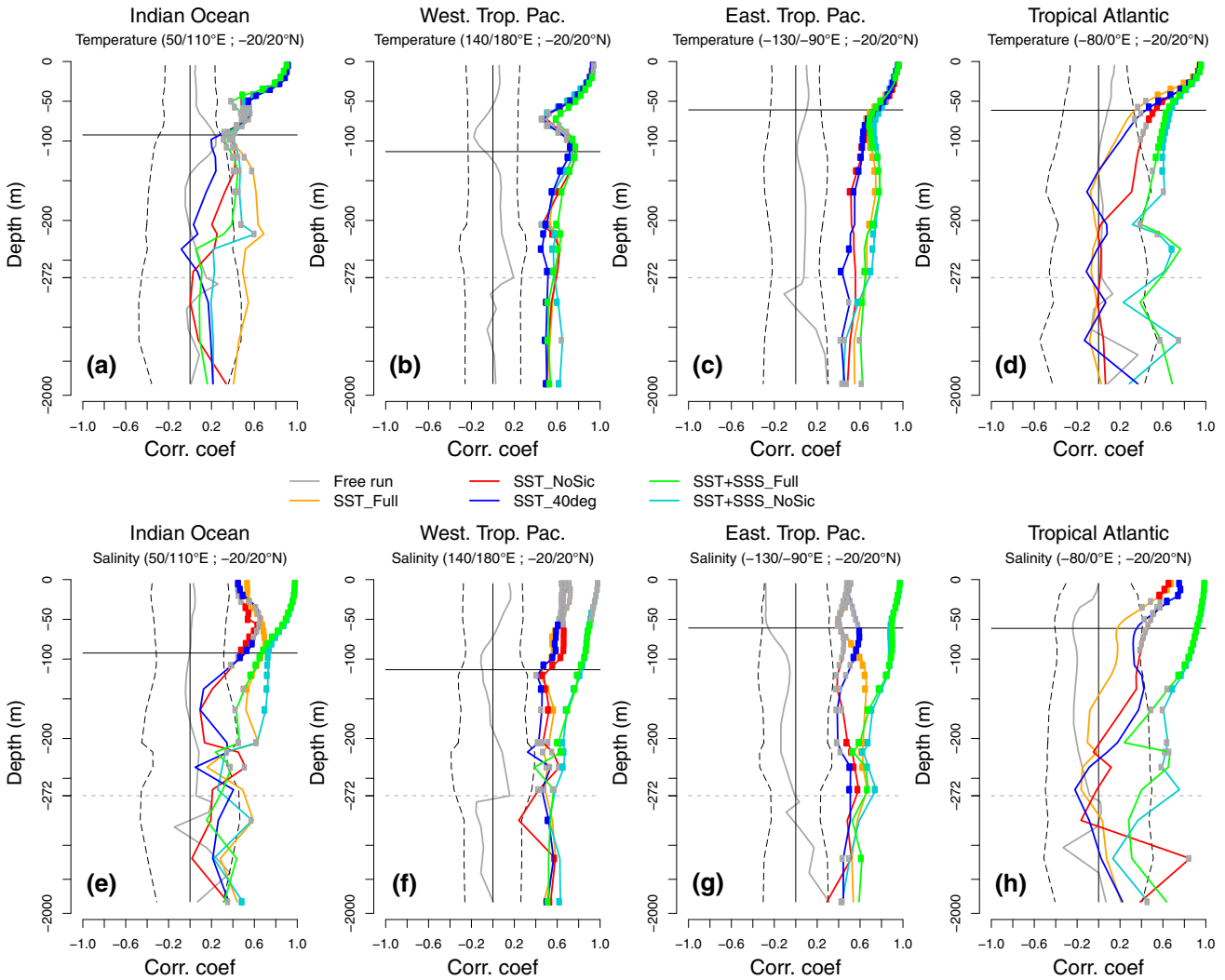

Fig. 5 Correlation between the nudged simulations (*colour solid lines*, see legend for the colour code), the free run (*grey solid line*) and the target with depth, for temperature (*upper row*) and salinity (*lower row*), and for the areas indicated at the *top* of each panel (tropical Indian: 50/110°E, −20/20°N, Western tropical Pacific: 140/180°E, −20/20°N, eastern tropical Pacific: −130/− 90°E, −20/20°N, tropical Atlantic: −80/0°E). The *dashed vertical lines* show the 99 % significance level for the correlation (Student *t* test taking into account the effective length of the time series). The *coloured circles* indicate the depths for which the correlation is significant (outside the *dashed* interval) and the Fisher F test not rejected (at 99 %). The *grey squares* highlight when the correlation is not different from the correlation between the free run and the target (test of difference between two Pearson correlation coefficients based on the Fisher transform, at 99 %). The *horizontal solid lines* show the mean depth of the 20 °C isotherm. The *horizontal grey dashed line* at −272 m indicates a change in the vertical scale

variance in the nudged simulations than in the target in the Southern Ocean and in the North Atlantic, south of Iceland. It is attributed to spurious convection occurring in the sea-ice border regions that trigger spuriously high variability (see above and below).

4 Influence of the surface nudging at depth

In this section we assess to what extent the surface restoring is able to reconstruct the subsurface temperature and salinity variability and explore the processes involved. For that purpose, correlations of vertical profiles of temperature and salinity are computed for different oceanic regions and for the 150 years of the simulations. As the processes involved are quite different, we analyse the tropics and the higher latitudes separately. The time series are detrended using the procedure detailed in the "Appendix". We focus on the first 2,000 m of the ocean, as deeper regions have too few degrees of freedom. For the mid- to high latitudes, results were unchanged when considering only a seasonal (winter or summer) analysis (not shown). The same correlation profiles were also done for the three consecutive 50-years periods (mimicking the length of the

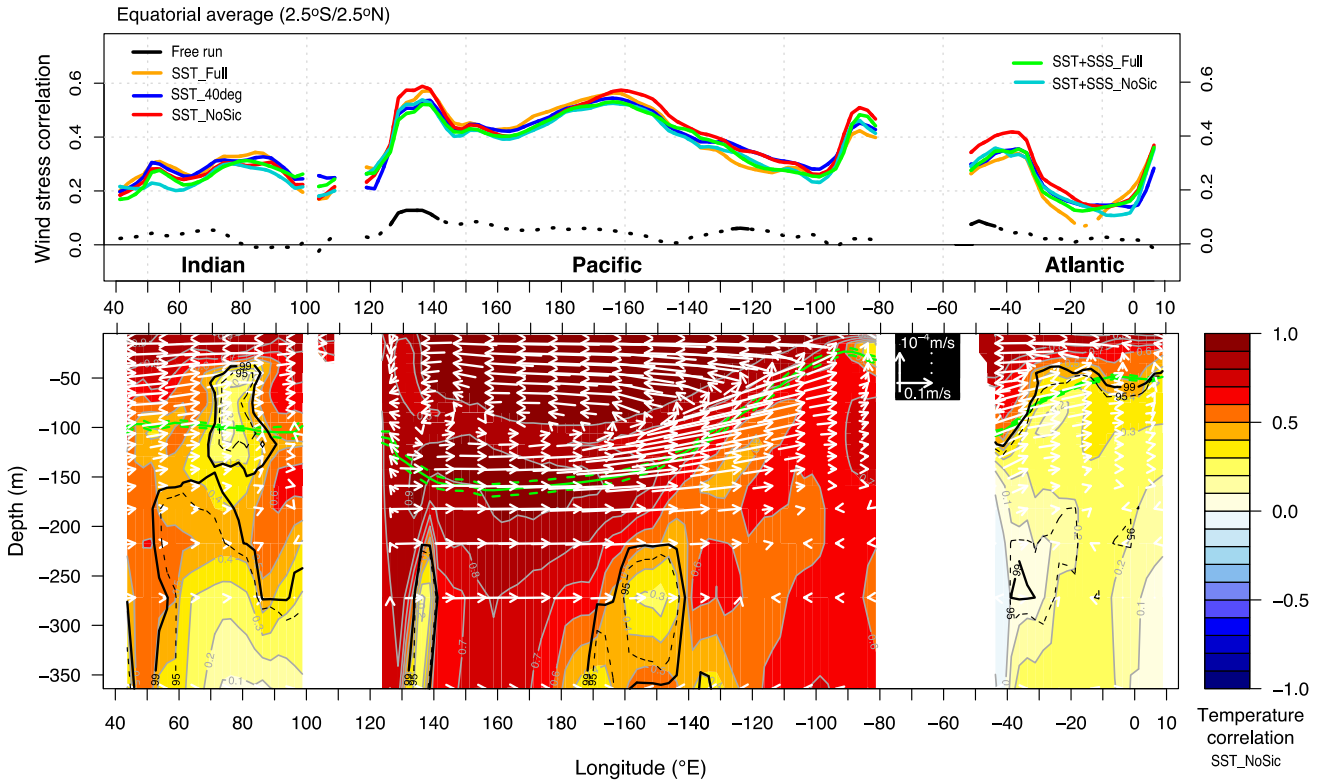

Fig. 6 *Upper panel* correlation coefficients of equatorial zonal wind stress (averaged between 2.5°S and 2.5°N) monthly anomalies (seasonal cycle removed), for the free run and all nudged simulations; *dotted lines* denotes correlations that are not significant at 99 % (Student *t* test). *Lower panel* correlation coefficient for the equatorial temperature as a function of depth (for SST_NoSic, shown as an example), averaged over the same latitudinal interval as for the zonal wind stress (*upper panel*). The *white arrows* show the climatological current velocity in the target run in the longitude-depth space (scale in the *black box*). The *thick solid black* contour highlights the correlation coefficients significant at 99 %, and the *thin black dashed* contour the correlation coefficients significant at 95 %. The *green* contours show the averaged mean (*solid line*) and plus or minus one standard deviation (*dashed lines*) of the depth of the 20 °C isotherm

observational period as done in Dunstone and Smith (2010)) and for five consecutive 30-years periods (not shown). No systematic deepening of the correlation with time was found, suggesting a rapid initialisation of sub-surface variability.

4.1 Tropical oceans

Figure 5 displays correlations between the nudged simulations and the target of vertical profiles for temperature (upper panels) and salinity (bottom panels) averaged over the tropical (20°S–20°N) Indian, the Western and Eastern tropical Pacific and the tropical Atlantic. The coloured circles indicate when the correlation is significant at the 99 % level and the ratio of the nudged simulation variance and the target one is not different from 1 (Fisher F test not rejected at the 99 % level).

In the tropical Pacific Ocean, the profiles for temperature (Fig. 5b, c) show significant correlation from the surface down to 2,000 m for all simulations. In this case, adding SSS nudging does not improve the correlation of temperature. As seen above and illustrated by the significant correlation from Fig. 5b, c and f, g, SST nudging in the tropical Pacific is enough to constrain the atmospheric circulation and the zonal wind stress (Fig. 6, top panel), with a direct effect on the slope and depth of the thermocline (Fig. 6, bottom panel) and the position of isopycnals down to 2,000 m. This is consistent with the results of Schneider et al. (1999) who have shown that the decadal temperature variability at depth in the tropical Pacific was largely controlled by the displacements of the isopycnals. It is also consistent with findings of Keenlyside et al. (2005) and Merryfield et al. (2010), two other studies using SST nudging in a coupled model and showing a significant impact on the winds and the subsurface ocean in the tropical Pacific. The temperature correlation displays a weaker value 50 m above the thermocline in the Pacific (see Figs. 5b, 6). More work is needed to understand the details of this feature but the advection of less well-reconstructed water from the subtropical cells may explain part of this distinctive signal. When SSS nudging is added, the salinity correlation is higher from the surface down to 250 m (R from 0.8 to 1) in both Pacific basins (Fig. 5f, g), suggesting that vertical diabatic processes also play a role

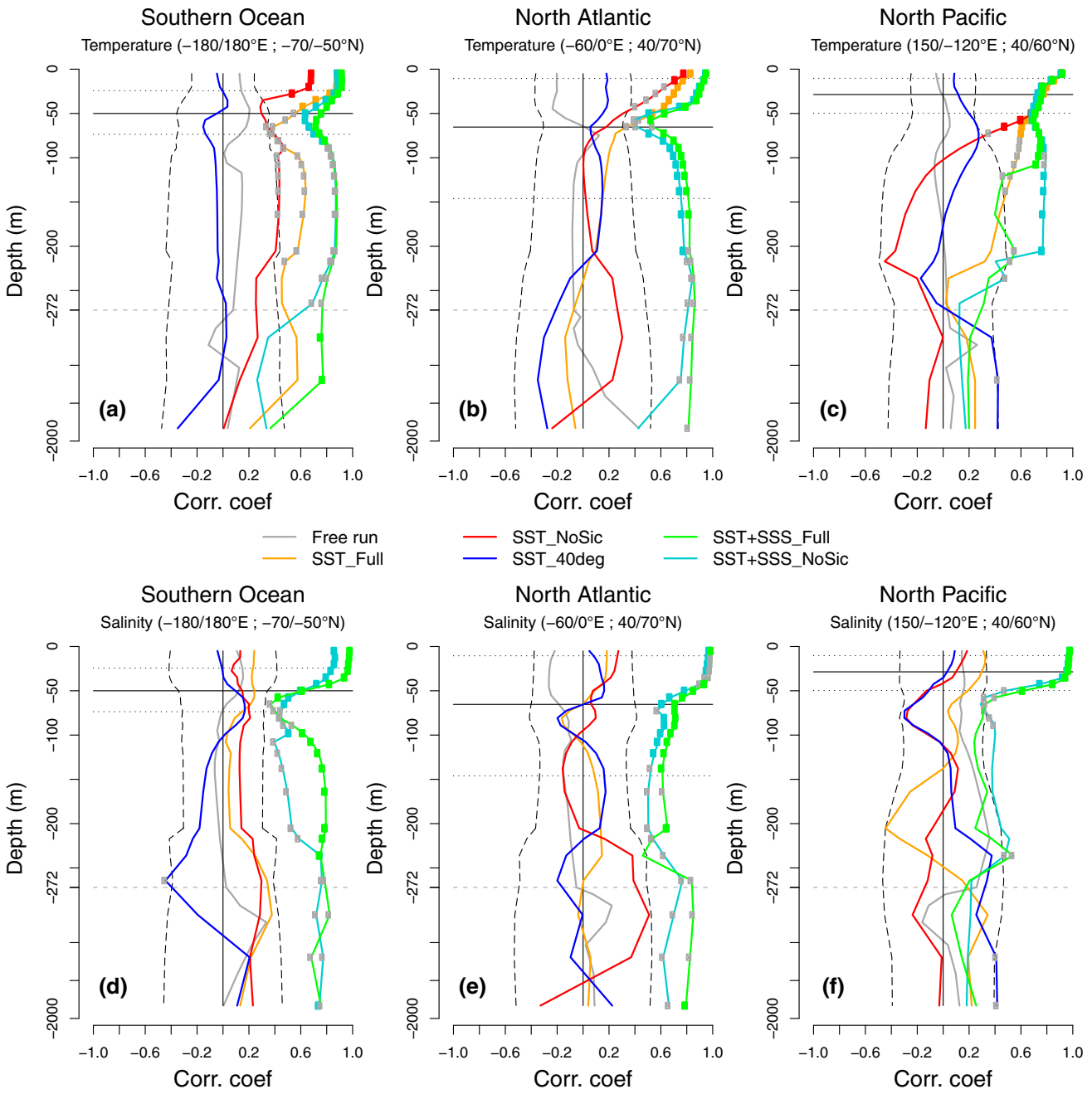

Fig. 7 As Fig. 5 for mid-to-high latitude areas (Southern ocean: −180/180°E, −60/− 40°N; North Atlantic: −60/0°E, 40/60°N; North Pacific: 120°E–120°W, 40/60°N). The *horizontal solid lines* show the annual mean depth of the 20 °C isotherm and the *dashed horizontal lines* the mean JFM and JJA depth of the 20 °C isotherm

in the reconstruction of the upper ocean, i.e. above the thermocline.

In the tropical Indian and Atlantic oceans the SST nudging is mainly able to reconstruct the temperature (Fig. 5a, d) and salinity (Fig. 5e, h) down to the mean thermocline (defined as the depth of the 20 °C isotherm, solid horizontal line). Nevertheless, we can see on Fig. 6 (lower panel) that the correlation signal in the equatorial Indian Ocean extends below the thermocline while it does not in the Atlantic Ocean. Given the complexity of the equatorial processes in the Indian Ocean, further investigation of this basin are deferred to a dedicated study. In the equatorial Atlantic, the influence of adjacent continents perturbs the reconstruction of the large-scale atmospheric circulation as compared to the Pacific (Fig. 4b and c), yielding a much shallower reconstruction of temperature. The SST nudging at the equator does not extend below the surface diabatic layers. Another argument is that modes of

variability in the Indian and Atlantic oceans, and associated anomalies, are primarily seasonal, only occurring a few months during the year (Xie and Carton 2004; Joly et al. 2007), unlike in the Pacific where ENSO dominates the annual mean anomalies. Adding the SSS nudging not only deepens the correlation of salinity well below the thermocline in the Tropical Atlantic but also that of temperature: significant correlation of both variables with the target reaches 150 m, which is about 100 m deeper than with SST nudging only. In the tropical Indian ocean, SSS nudging has no impact on SST correlation (Fig. 5a).

4.2 Mid- to high latitudes

Figure 7 displays vertical profiles of correlation between the nudged simulations and the target for three high latitude regions, the Southern Ocean, the North Atlantic and the North Pacific, together with the mean and seasonal mixed-layer depth. As expected from the processes involved at these higher latitudes, there is a stronger contrast between the simulations with and without SSS nudging than in the Tropics.

In SST_Full and SST_NoSic (i.e. just using SST nudging), significant temperature correlations are shallower than 100 m (i.e. mostly in the summer mixed-layer—upper dotted line—in the Southern Ocean and in the North Atlantic, and reaching just below the winter mixed-layer—lower dotted line—in the North Pacific). The salinity is not initialised in these simulations (correlations are not significant at the 95 % level) as, in contrast to the Tropics, air–sea interactions are not strong enough at these latitudes to constrain the atmospheric freshwater fluxes. SST_40 deg has no significant correlation for temperature or salinity at these latitudes. This is expected as no direct nudging is applied, but it also indicates that poleward advective processes (from the tropics where the SST is nudged) are either not sufficient to reconstruct the subsurface or that they involve deeper layers that are not reconstructed in the tropics.

In simulations where both the SST and SSS are nudged, both temperature and salinity correlations extend much deeper, reaching 2,000 m in the North Atlantic and in the Southern Ocean. These are regions of active deep convection, a central process to form water masses in the ocean interior, in which salinity plays a key role via its impact on density and buoyancy forcing (Swingedouw et al. 2007a). Spearman ranking correlation maps of mixed-layer depth (MLD) in the North Atlantic and for the winter season are shown for SST_Full, SST_NoSic, SST + SSS_Full and SST + SSS_NoSic in Fig. 8. The winter MLD in the model's deep convection sites, as defined by Escudier et al. (2013), is much better reconstructed in simulations with SSS nudging (correlation up to 0.9) than in simulations without, in which the MLD correlation is not significant north of 40°N. The MLD variance is also overestimated (Fig. 8), likely due to the spuriously large SST-nudging-driven intermittent buoyancy forcing discussed in the introduction and further explored in Sect. 6. In the North Pacific, as no deep convection is present, the processes involved in the reconstruction are restricted to the upper layers. Significant temperature correlations reach 100 m (i.e. 50 m below the winter mixed-layer) and the salinity is reconstructed down to the winter mixed-layer when SSS is also nudged.

The correlation of vertical profiles for the rest of the ocean (mostly the 40–20°S and 20–40°N latitudinal bands) exhibits temperature and salinity reconstruction down to about 250 m (not shown), likely reflecting the influence of the ventilation pathways associated to the western boundary currents.

In summary, surface nudging is able to reconstruct ocean interior temperature and salinity at mid-latitudes via the main mechanisms involved in water mass formation: surface buoyancy forcing, deep convection and thermocline ventilation. To get additional physical insights on the impact of surface nudging, which directly affects the surface buoyancy forcing, we now perform a water mass transformation (WMT) analysis following Walin (1982) and Speer and Tziperman (1992). By projecting the variables and processes on density, the ocean natural coordinate, this diagnostic highlights the diabatic processes that transform water masses, namely surface buoyancy forcing and diapycnal diffusion. Here we concentrate on the surface buoyancy forcing associated with surface heat and fresh water fluxes to further understand the impact of SST and SSS nudging.

For a given region and for each simulation, the monthly WMT anomalies (i.e. seasonal cycle removed) are computed as a function of potential density and time, e.g. $WMT(\sigma_0, t)$. Those WMT anomalies are a quantification of the water mass fluxes (in Sv) across isopycnals due to surface heat and freshwater forcing and their impact on surface density. The correlation of WMT time series between each nudged simulation and the target is then computed across all densities (isopycnals) and time (Fig. 9). The analysis is performed for the total WMT as well as the thermal and haline components in the mid-latitude regions assessed above. This WMT metric provides a synthetic measure of the agreement of the total water mass transformed through all isopycnals over a given region by giving more weight to the isopycnals and the seasons that exhibit high WMT variance (Speer et al. 2000; Speer and Tziperman 1992).

In the Southern Ocean and in the North Pacific, local SST nudging (i.e. SST_Full and SST_NoSic) already provides a 0.1–0.2 increase in correlation of total WMT over

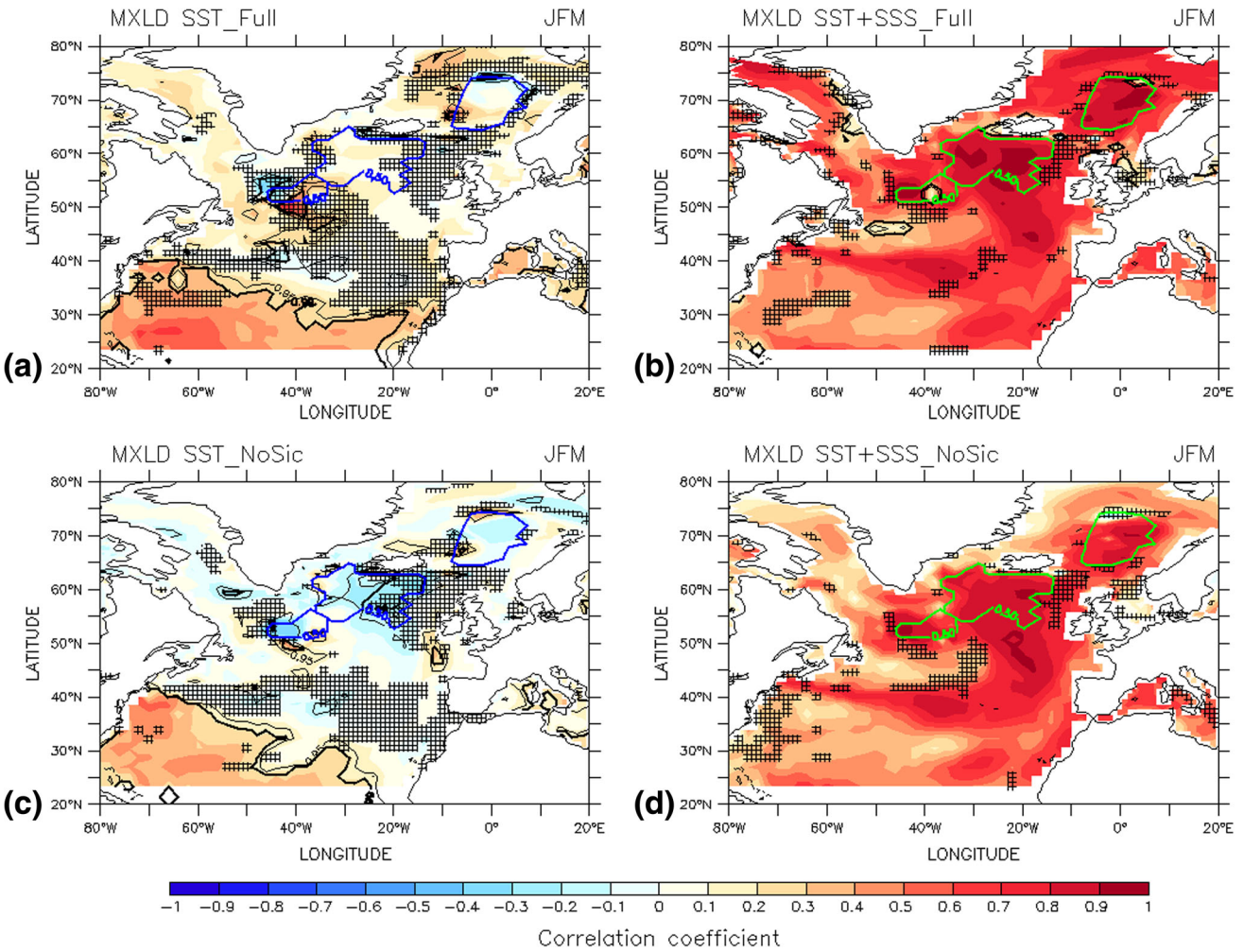

Fig. 8 Spearman rank correlation maps for the winter (January–February–March, JFM) MLD in SST_Full (**a**), SST + SSS_Full (**b**), SST_NoSic (**c**) and SST + SSS_NoSic (**d**) in the North Atlantic. The *thin* and *thick black contour lines* highlight the 95 and 99 % significance level for the correlation. The hatching shows where the Fisher F test is significant at more than 99 % confidence level (with standard deviation ratio greater than one). The *blue* contours in panels **a** and **c** and the *green* contours in panels **b** and **d** depict the deep convection sites described in Escudier et al. (2013) in the IPSL-CM5A model (*different colours* for display convenience)

SST_40 deg, which, as expected, exhibits no correlation (Fig. 9). Nudging to SSS has a very large impact, driving the correlations of total WMT to values between 0.4 and 0.6 in all regions. The impact is stronger in the North Atlantic and in the Southern Ocean than in the North Pacific and contributes to explain the better reconstruction (deeper and with higher correlation coefficient) of temperature and salinity at depth in those regions (seen on Fig. 7). The thermal and haline components contribute equally to this improvement. The direct impact of SSS nudging on the haline component is straightforward. By reconstructing the correct location of isopycnals at the surface, SSS nudging also allows the correct heat flux (i.e. that of the target) to transform the correct surface density, hence also improving the correlation of the thermal component of the WMT. This is especially the case in the North Atlantic (Fig. 9) where the deep convection sites are reconstructed (Fig. 8). It should be noticed that WMT variance in the North Atlantic is larger than in North Pacific due to very different processes in these two basins (notably convection in the Atlantic). This difference certainly affects the correlation and may explain different performances between the Atlantic and the Pacific among the simulations.

5 Reconstruction of the AMOC

5.1 AMOC index in the target and the simulations

The AMOC index is defined as the maximum of the Atlantic meridional stream function from 500 m to the bottom and between 20°S to 60°N. It is shown for the different nudged simulations (Fig. 10b–f) and the free run (Fig. 10a) compared to the target (black curve in Fig. 10a–f). The target

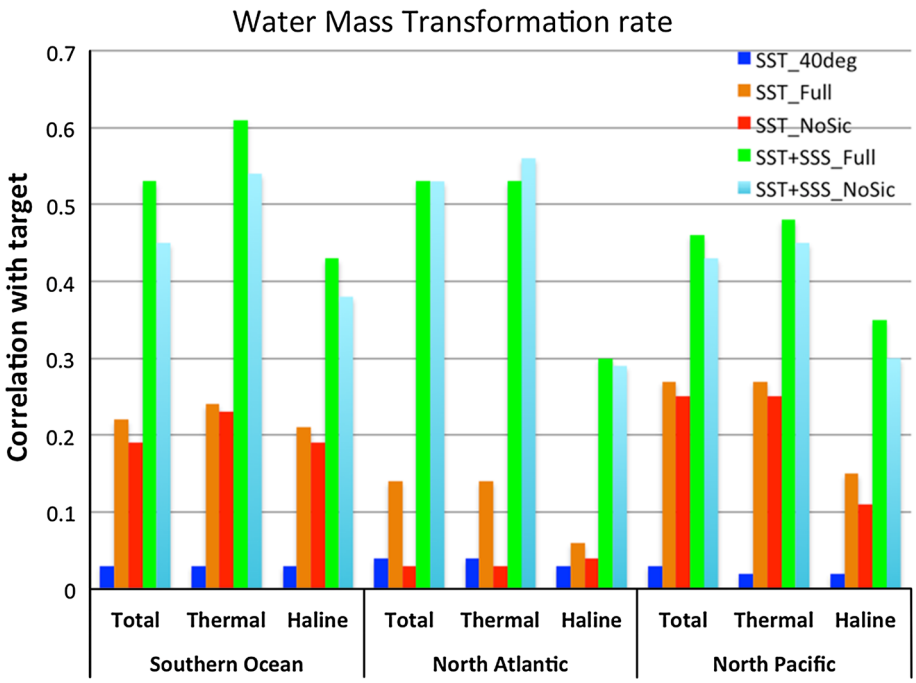

Fig. 9 Correlation of the total water mass transformation rate and its thermal and haline components, between the five nudged simulations and the target, for the 3 mid-latitudes regions shown in Fig. 7

AMOC index time series shows two large anomalies between 2,230 and 2,270 (~4 Sv in 2,240 and ~2 Sv in 2,260, while the standard deviation is of 1 Sv on the 150 years considered), separated by roughly twenty years, consistent with the bidecadal periodicity in the subpolar North Atlantic described by Escudier et al. (2013) in this model (further detailed below). After 2,270 and before 2,230, the variability of the target AMOC index remains close to plus or minus one standard deviation (as estimated from the 1,000-year control simulation). The agreement between the simulations and the target is assessed using both a 31-year moving correlation of the annual mean AMOC (right hand-side axis) and the 150-year correlation (value given on panel). The results are similar if a 5-year filtered AMOC time series is used.

Nudging only to SST allows reproducing the two large AMOC peaks between 2,230 and 2,270 (see grey shading of the moving correlations in Fig. 10b, c, d) but the 150-year correlation is not significant. In SST_40 deg, the two AMOC peaks are reproduced but their amplitude is lower by 1 or 2 Sv as compared to the target. In SST_NoSic, the first peak matches that of the target both in terms of correlation and amplitude and the second one is larger by more than 1 Sv. The AMOC index of SST_Full shows continuous and stronger variability compared to the target. Adding the SSS nudging (SST + SSS_Full and SST + SSS_NoSic, Fig. 10e, f) significantly increases the AMOC index correlation for the whole 150-year period ($R = 0.59$, significant at the 95 % level) and multiplies by 3–4 the duration of the period with significant 31-year moving correlation.

5.2 Origin of the AMOC reconstruction

Escudier et al. (2013) have shown that in the IPSL-CM5A-LR model winter deep convection in the subpolar North Atlantic (notably in the three model convection sites depicted on Fig. 8), mainly triggered by salinity anomalies, is a major driver of the AMOC.

Using their analysis framework we first explore why SST_Full exhibits continuous and stronger AMOC variability when compared to the target. This spurious behaviour is not seen in SST_40 deg and SST_NoSic and is attributed to spurious convection near the sea-ice edge in SST_Full. As illustrated on Fig. 11 for a situation that develops between the first and fourth winters after the beginning of the nudging, when a region is covered by sea ice in the target and not in SST_Full, the resulting negative heat flux correction is anomalously high (reaching 100 W/m^2 and more). This produces dense cold water at the surface that trigger spurious convection in winter in SST_Full (Fig. 11) and thus induces an anomalous strengthening of the AMOC, while such convective event does not occur in the target. As for real convective events, this behaviour is not necessarily instantaneous, and the spurious convection may require two or three consecutive winters with such sea-ice border mismatch and intense surface cooling to be triggered. Using a more sophisticated method of coupled assimilation but incorporating only atmospheric data and SST, Zhang et al. (2010) obtained a reasonable correlation between the target AMOC and the reconstruction ($r = 0.85$), but they also found a poor reconstruction of the water mass

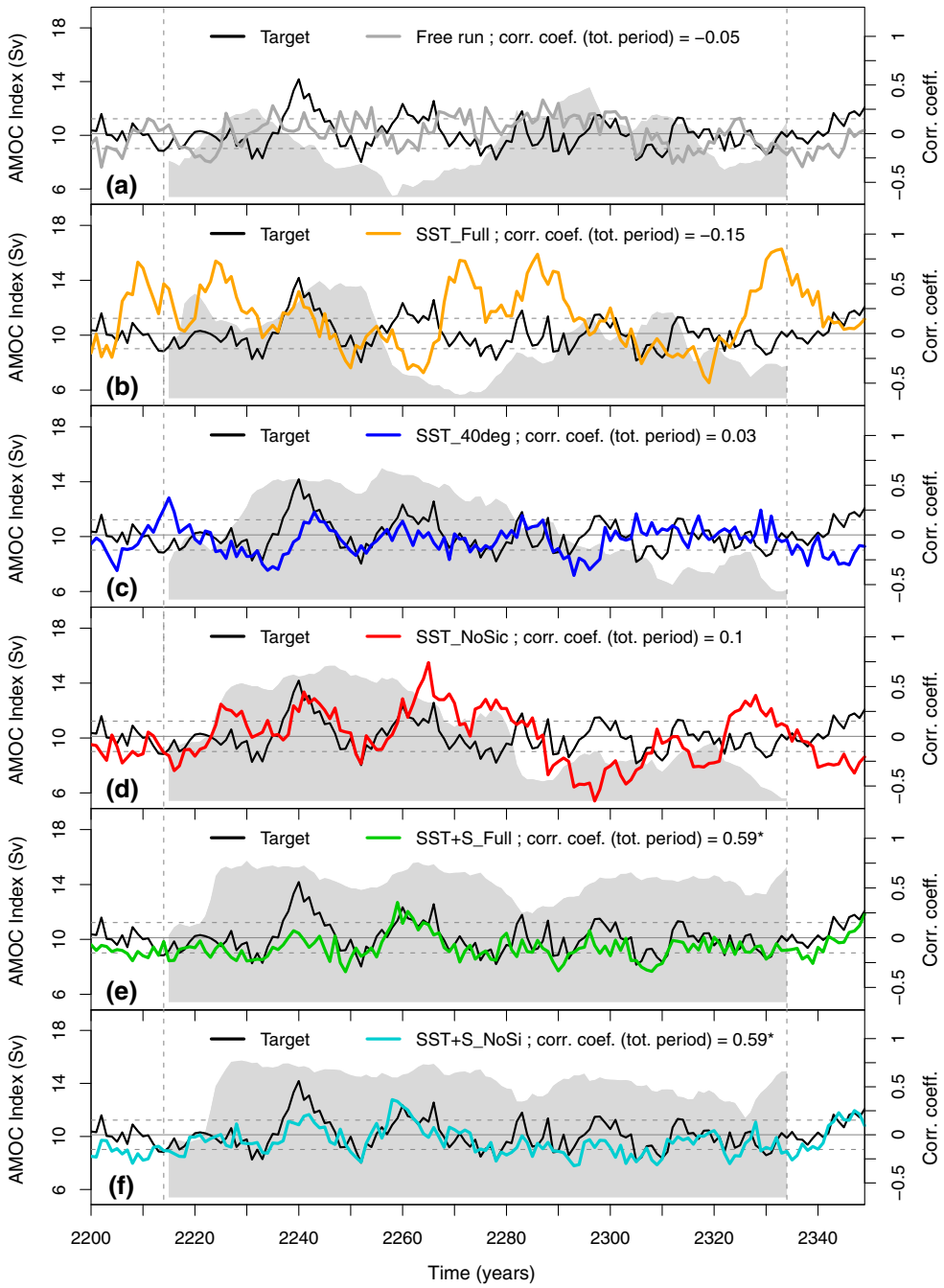

Fig. 10 AMOC index in the target period (*black solid line*), the free run (*dashed grey line*) and the different nudged simulations (*solid coloured lines*). The correlation coefficients estimated between the target and the nudged simulations on the whole period are written in the legend for each panel. The * indicates that the correlation is significant at 95 %. The *shaded* background is the moving correlation (31 year-window) between the target and the different simulations; the *dark grey* background shows the correlations that are significant at 95 %. The *horizontal solid line* shows the target mean and the *two horizontal dashed lines* depict plus or minus one standard deviation of the target

originating from convection on the Greenland Sea. An interesting point is that, considering the same winters as in SST_Full, this spurious convection event does not occur in SST + SSS_Full (Fig. 12). Moreover, we found no anomalously strong convection event in the three main North Atlantic deep convection sites [defined in Escudier et al. (2013)] in SST + SSS_Full while events that drastically exceed the target variability occurred at multiple occasions in SST_Full (not shown). It suggests that the anomalous buoyancy fluxes triggered by the SST nudging are sufficiently compensated by the buoyancy fluxes due to the SSS nudging to avoid these spurious high convection events in winter in this region.

To further understand the reconstruction of the two major AMOC peaks in SST_40 deg and SST_NoSic and the improved overall correlation in SST + SSS_Full and SST + SSS_NoSic, we follow the analysis of Escudier et al. (2013). The mechanism involved an intensification of the East Greenland Current (EGC), which transports additional cold and fresh water in the Labrador Sea where it accumulates and leads to negative SST and SSS anomalies. These anomalies are then advected along the

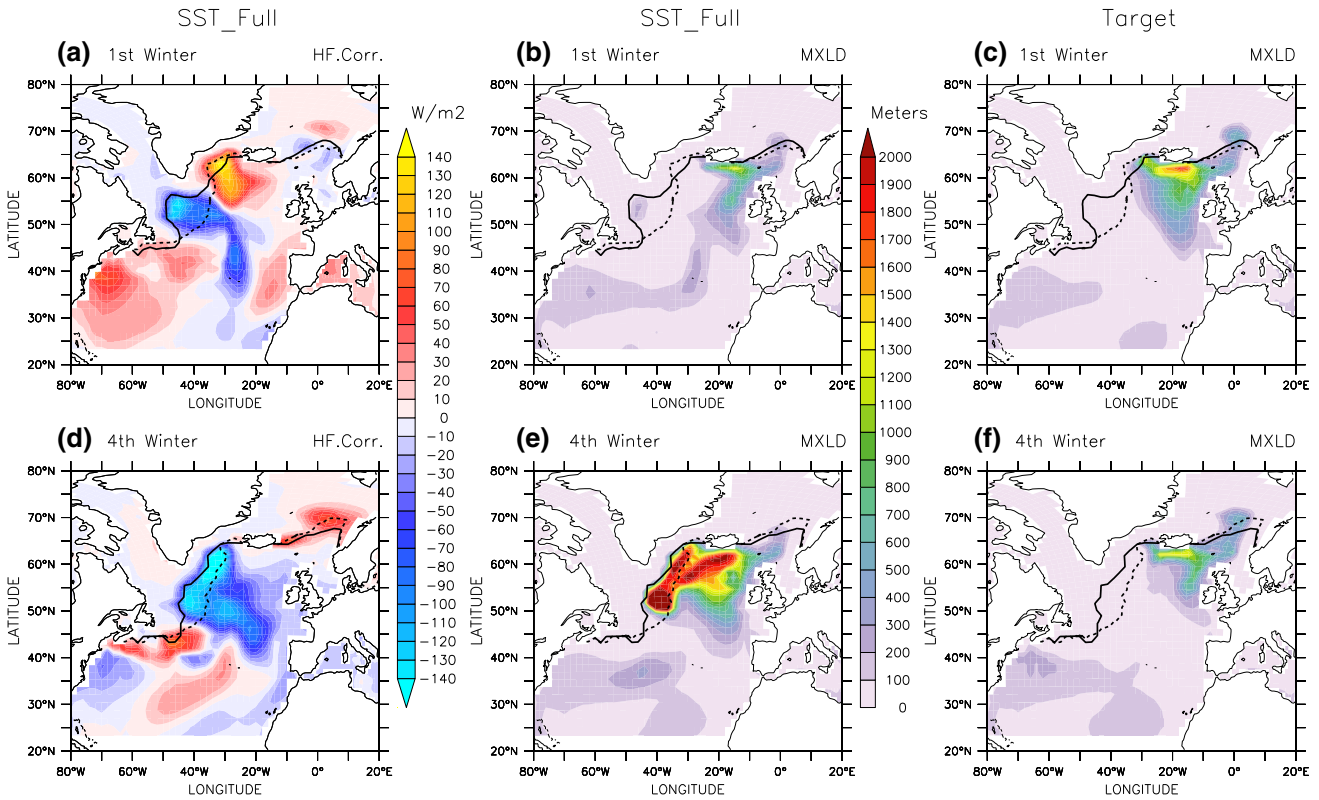

Fig. 11 *Left column* restoring heat flux correction (unit: W/m^2) for winter (JFM) 2201 (**a**) and 2204 (**c**) in SST_Full; *middle* and *right columns* mixed-layer depth (unit: m) in SST_Full (**b**, **e**) and the target (**c**, **f**) for the corresponding first and fourth winters. Contours denote the sea-ice border (0.01 sea-ice fraction isoline) in SST_Full (*solid contour*) and in the target (*dotted contour*)

subpolar gyre; they affect the convection all along their path up to the Nordics Seas, where the negative SST anomalies increase the sea-ice cover, which in turn induces a positive sea-level pressure anomaly and a localised anti-cyclonic atmospheric circulation. This leads to a decrease in the wind stress along the eastern coast of Greenland and thus a weakening of the EGC, leading to the opposite phase of the cycle about 10 years after its initiation. This cycle influences the AMOC through the impact of the propagating SSS anomalies on the convective activity in the northern North Atlantic. Indices associated to this sequence in the nudged simulations are compared to that of the target in Fig. 13 (SST_40 deg and SST_NoSic) and in Fig. 14 (SST + SSS_Full and SST + SSS_NoSic). In SST_40 deg, no restoring happens north of 40°N. To assess whether the salinity, which is reconstructed in the tropical Atlantic (Sect. 3.2) and then transported northward by the ocean circulation (e.g. Mignot and Frankignoul 2009), can play a role, the northward salt transport through a section crossing the North Atlantic at 45°N (−60 to −20°E), extending down to 500 m in depth is added to the above indices (Figs. 13b, 14b). This would provide an alternative mechanism to explain the origin of salinity anomalies in the subpolar North Atlantic triggering deep convection.

The first AMOC peak in the target (black curve Fig. 14h, year 2240) is preceded by a convection maximum in the Western site (see Fig. 8 and Escudier et al. 2013 for further definition) by about 6 years (year ∼ 2234, Fig. 13d), then by a convection maximum in the Southern site (year ∼ 2236, Fig. 13e) and finally by a convection maximum in the Northern site (year 2238–2239, 2 years before the AMOC peak, Fig. 13g). These timescales are coherent with the findings of Escudier et al. (2013). Before this sequence of convective events, the averaged salinity in the first 200 m (S200) of the Labrador Sea exhibits a maximum (∼2228, Fig. 13c). Figure 13a shows that this subsurface salinity maximum can be triggered by a deceleration of the EGC (with a minimum around year 2222, Fig. 13a) as in Escudier et al. (2013). Yet, Fig. 13b does not allow ruling out a possible influence of the tropics, as an increase of the northward salt transport at 45°N (with a maximum around year 2223, Fig. 13b) could also induce the salinity maximum. This result thus highlights a possible competitive mechanism to the one described in Escudier et al. (2013). Note however that in the target, the maximum of northward salt transport at 45°N is not particularly strong compared to the variability on the whole period. Furthermore, the role of the variability of the Northward

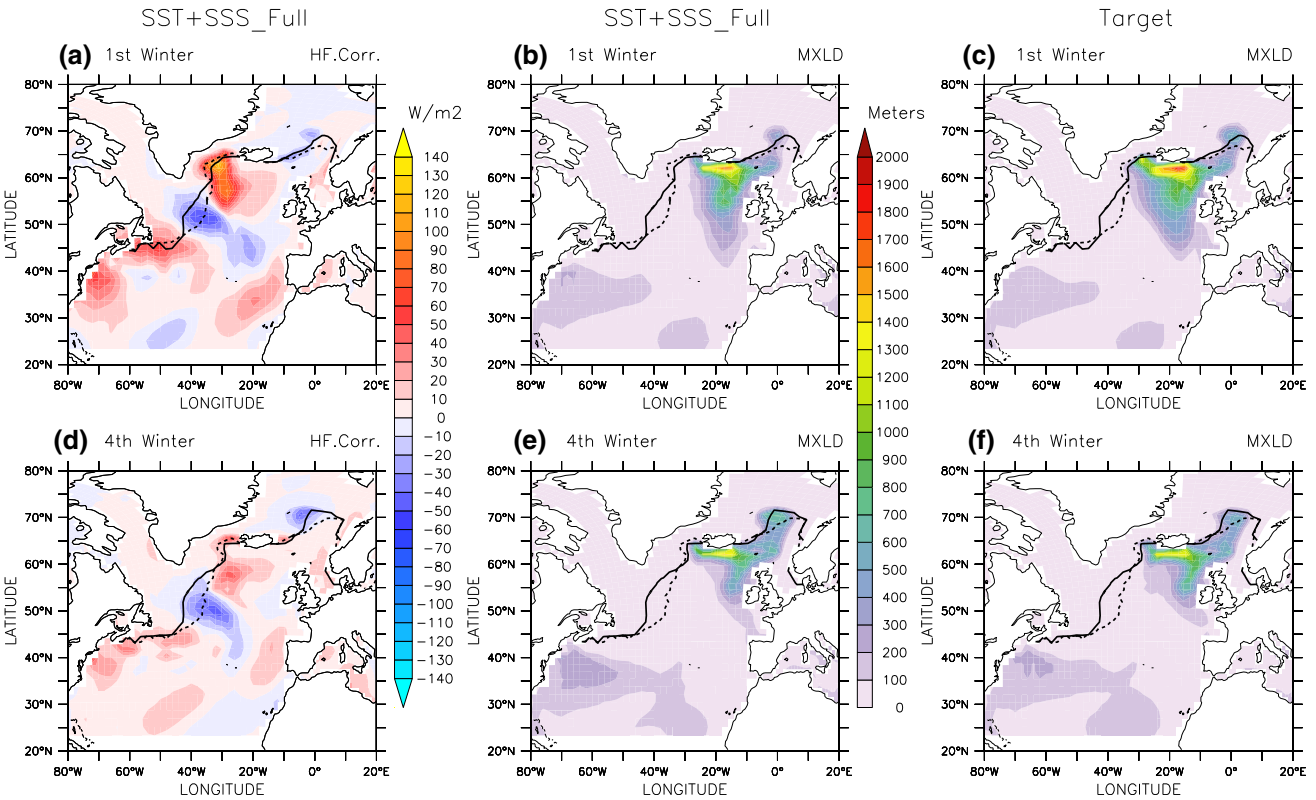

Fig. 12 Same as Fig. 11 with SST + SSS_Full in place of SST_Full

salt transport on the AMOC variability is complicated because this poleward salt transport is also partly driven by the AMOC circulation itself (e.g. Goelzer et al. 2006; Swingedouw et al. 2007b). Investigating in details this mechanism is beyond the scope of the present paper. A similar chain of events and lags can be seen for the second target AMOC peak of year 2260.

The target subsurface salinity (S200) maxima discussed above (years 2228 and 2247, Fig. 13f) are reproduced to some extent in SST_40 deg, although with a lower intensity. Consistently, this simulation captures the two large AMOC peaks, but with a lesser amplitude. The EGC spin down around year 2222 in the target is not simulated in SST_40 deg. The deep convection events in the southern and northern sites (associated with the first AMOC peak) are rather due to the anomalous northward salt flux at 45°N, which follows quite closely that of the target (Fig. 13e, g, b). This performance of SST_40 deg is notable and the current hypothesis is that the salinity anomalies in the Northern convection site are associated to the maximum of Northward salt flux at 45°N around year 2222.

In SST_NoSic (Fig. 13), the S200 maximum in the Labrador Sea (year 2228 in the target) is reproduced with a delay of about 4 years. It is also lower than in the target by $\sim$0.2 psu. Nevertheless, it leads to the reconstruction of the successive convection maxima in the three convection sites. The second AMOC peak in SST_NoSic has larger amplitude than in the target, although the series of event prior to deep convection is very similar to that of the target. The larger convective signal is possibly due to the strong heat flux corrections close to the sea-ice border previously discussed as the SST $>$ 0 criteria may not be totally effective in this complex region.

In both SST + SSS_NoSic and SST + SSS_Full all indices of the 20-year cycle follow quite closely the target (Fig. 14). Deep convection in the Western site in 2232 is underestimated in both simulations (Fig. 14d), which might explain the underestimation of the first AMOC peak in 2230 (Fig. 14h).

The Northward salt flux in both simulations also mainly reproduces the evolution of the target, apart from the maximum around 2240, due to the underestimated concurrent AMOC peak. Compared to SST_NoSic and SST_Full, no spuriously high convection occurs in the simulations with restoring to SST and SSS. It thus suggests that the value of γ_S used here sufficiently counterbalances the buoyancy flux due to the SST nudging near the sea-ice edge to avoid those spurious convection events.

In all nudged simulations, the correlation of the AMOC index is not significant during the first 25 years. This is interpreted as the time needed to initiate the mechanisms described above, to the weak variability of the target in the

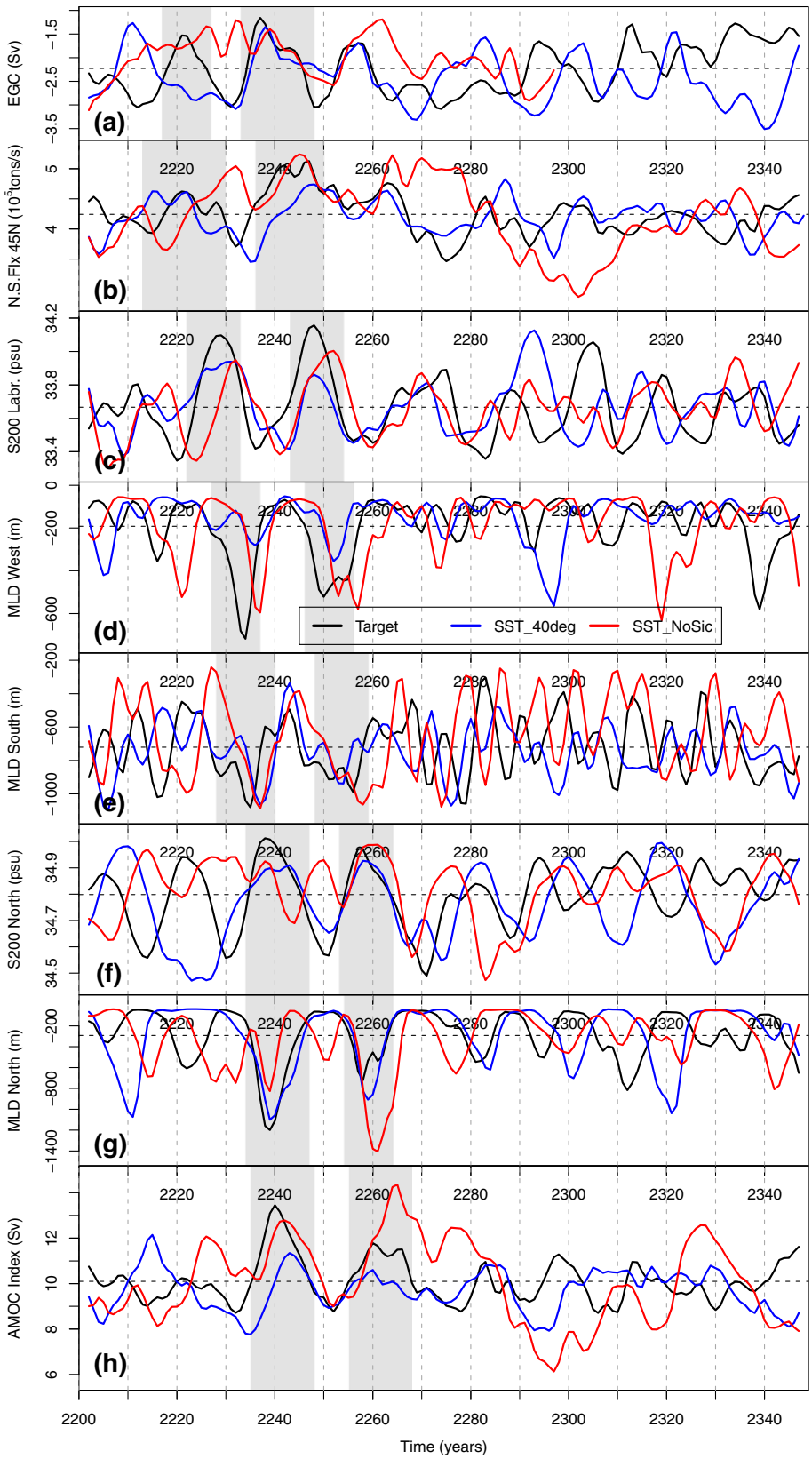

Fig. 13 *Bottom panel* (**h**) AMOC indices of the target (*black solid line*), SST_NoSic (*red solid line*) and SST_40 deg (*blue solid line*); the colour code is the same for all panels; on panels **a**, **c**, **d**, **e**, **f**, **g**, and **h** are shown the indices of the phenomenon at play in the 20-year cycle described by Escudier et al. (2013): the EGC index (**a**), the salinity averaged over the upper 200 m (S200) in the Labrador Sea (**c**), the Mixed Layer Depth (MLD) in the Western (**d**), Southern (**e**) and Northern (**g**) convection sites, and the S200 in the Northern convection site (**f**). On panel **b** is represented the Northward salt flux (unit: 10^5tons/s) through a zonal section extending from −60 to −20°E, and down to 500 m deep. The *horizontal dashed lines* represent the mean of the target on each panel. The two first *vertical thick grey lines* highlight the event for each index identified to be at the origin of the first AMOC peak (between 2,235 and 2,248). Same for the two next *vertical thick grey lines* with the second AMOC peak (between 2,255 and 2,268). All the indices have been smoothed with a 5-year Gaussian filter

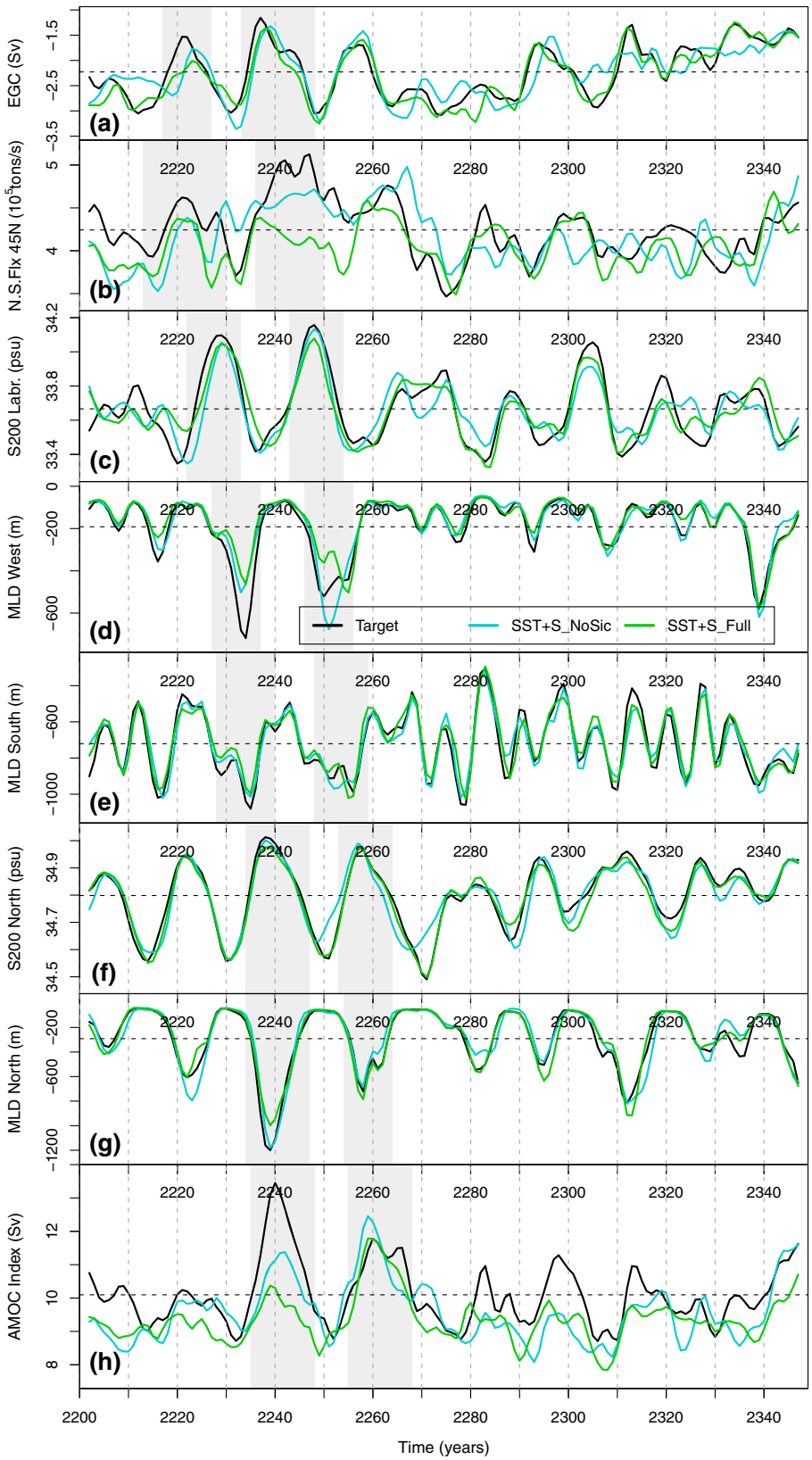

Fig. 14 Same as Fig. 13 but for SST + SSS_NoSic (*light blue solid line*) and SST + SSS_Full (*green solid line*)

first 25 years, or to both. In any case, and after these 25 years, the reconstruction of the AMOC does not improve with the amount of time spent nudging. There are rather periods when the reconstruction via surface nudging is efficient, and periods when it is not.

6 Conclusion

Initialising the internal variability of models for decadal predictability studies and hindcasts is a new area of research and a variety of *ad hoc* methods are proposed to initialise the ocean, i.e. the slow component of climate. In this study, we explore how SST and SSS surface nudging can reconstruct the three-dimensional variability of the ocean in a perfect model framework. The motivation for using surface nudging only is to drive the model towards the observed trajectory while keeping internal dynamics, a major source of predictability, coherent. This strategy builds on the fact that oceanic processes themselves will transport the surface information into the ocean interior as seen in ocean-only simulations. When transposed out of the perfect model framework, this strategy is also motivated by the higher reliability of surface time series compared to subsurface data and reanalysis. To further keep physical consistency, the restoring coefficients for SST used here is of the same order as the heat-flux feedback estimated from observations, in contrast to previous related studies, which used O(10) larger values.

Five nudged simulations are designed to reconstruct a 150-years "target" simulation, defined as a portion of the 1,000-years IPSL-CM5A-LR pre-industrial CMIP5 control simulation (Fig. 2; Table 1). The nudged simulations differ by the variables restored to (SST or SST + SSS) and by the area where the nudging is applied, namely to deal with the restoring at high latitudes and near sea-ice border.

SST nudging is able to reconstruct the mean mixed layer temperature where it is applied, even with the "weak" physically based restoring coefficient used here. Where the advection processes also drive the SST or when the heat fluxes counterbalance the surface nudging, the correlation of the variability with that of the target is weaker (e.g. mid- to high latitudes, west border currents). In the tropics, SST nudging alone also reconstructs the SSS via the hydrological cycle. SSS nudging is enough to fully reconstruct the SSS over the whole globe. It also improves the SST reconstruction at mid- to high-latitudes.

Away from the surface, the vertical profiles of the correlation and variance ratio of the nudged simulations with the target show that the subsurface reconstruction depends on the latitude (Figs. 5, 7) and can be traced back to the dynamical and diabatic processes controlling the ocean circulation. SST nudging is efficient at reconstructing the tropical regions (30°S–30°N), and less so at mid-to-high latitudes. Tropical SST is a strong driver of the atmospheric circulation. Nudging the SST in this region is able to reconstruct the convergence and divergence zones and their variability, and the associated vertical motions, as illustrated from surface wind and the evaporation-precipitation patterns. In the Pacific Ocean, equatorial temperature profiles show a significant correlation from the surface down to 2,000 m for all simulations (Fig. 5b, c, f, g). In contrast, the significant correlation in the equatorial Atlantic is restricted to the region above the thermocline. This difference comes from the wind variability reconstruction in the Pacific that contributes to a dynamically driven reconstruction in addition to the surface driven diabatic source. In the Atlantic, the coupling between the winds and zonal gradient is not as strong as in the Pacific, so that such a dynamical adjustment and reconstruction of the temperature profile is not present.

At mid-to-high latitudes, SSS nudging is required to reconstruct both the temperature and the salinity below the seasonal thermocline. This is particularly true in the North Atlantic where adding SSS nudging is able to reconstruct the oceanic deep convection regions of the target. A water mass transformation analysis is used to quantify the impact of the heat and fresh water fluxes associated to surface nudging. Beyond the straightforward impact on the haline component, SSS nudging also improves correlation of the thermal component. This is due to reconstruction of the location of isopycnals at the surface hence allowing the heat flux to transform the correct surface density. This contributes to the deeper reconstruction of both temperature and salinity variability in the mid-to-high latitudes regions.

Restoring to SSS significantly improves the reconstruction of the AMOC variability, with significant correlation for more than 80 years in SST + SSS_Full and SST + SSS_NoSic, compared to less than 30 years otherwise. In the nudged SST simulations only the large AMOC anomalies are reproduced. This is achieved by reproducing the timing of the processes that control the 20-year AMOC cycle in the model, as described by Escudier et al. (2013). This distinctive mode of variability is a potential source of initialisation of the AMOC as also found in Swingedouw et al. (2013). Advection of reconstructed salinity anomalies from lower latitudes is also proposed as an additional mechanism for reconstructing the AMOC. This is particularly interesting as tropical salinity anomalies are indirectly reproduced through air–sea interactions in the Tropics. This mechanism seems to be at play episodically in the simulation with no restoring poleward of 40°.

When SSS nudging is added, deep convection events are much better reconstructed and this explains the better

reconstruction of the AMOC. The reconstruction of SST and SSS in the subpolar Atlantic region in the simulations with SSS nudging strongly suggests that the surface buoyancy fluxes are well reconstructed, which explains the correct reconstruction of the winter variability of the deep convection in this region. Nonetheless, the amplitude of the first major AMOC peak (around 2240) is not fully reproduced, even with SSS nudging. This peak is actually an extreme AMOC peak (above the 95th quantile of the distribution of the AMOC variability in the 1,000-year simulation) and likely due to a combination of factors (buoyancy fluxes but also wind forcing). The fact that the surface buoyancy fluxes are not perfectly reproduced may explain that the amplitude of the AMOC and MLD West peaks is partially misrepresented. Furthermore, we expect that the wind, not reconstructed in the North Atlantic region (neither by nudging or by indirect reconstruction), could play a role in the large amplitude of both the AMOC peak and the preceding MLD West convective event in target simulation. This question is currently investigated with a dedicated study of the causes of these extreme events and will be reported in a subsequent study.

The spurious convection events driving the anomalously high AMOC variability in the SST-only nudged simulations are not present in the simulations with SSS nudging. This suggests that the strong negative heat fluxes linked with SST nudging are sufficiently compensated in terms of buoyancy flux by the SSS nudging to prevent the spurious convection events. Given the climate impact of AMOC variability (e.g. Latif et al. 2006; Zhang and Delworth 2006), the potential predictability of the AMOC (Msadek et al. 2010; Persechino et al. 2013) and therefore the importance of the AMOC reconstruction for decadal predictions, SSS nudging in addition to SST nudging appears as a crucial improvement in a surface nudging strategy for further improving the AMOC reconstruction in the real world (Swingedouw et al. 2013).

The NoSic configurations were designed to avoid problems linked with spurious convection in the sea-ice border regions. Compared with SST_Full, the variability of the AMOC in SST_NoSic was closer to the target (both in terms of amplitude and phase) but still, anomalous convection has been evidenced in SST_NoSic as well as an overestimated AMOC variability. There was no real difference between the Full and NoSic configurations for the simulations with both SST and SSS nudging.

For both SST and SSS nudging, the surface (and mixed layer) reconstruction is effective within the first year, coherent with a relaxation time of 2 months for the restoring coefficients used. Beyond this rapid initial adjustment, no systematic and durable improvement of the quality of the reconstruction with time could be identified for temperature and salinity at depth (moving correlation, or correlations over successive 50-year periods were used). There are rather periods/events when the reconstruction via surface nudging is efficient, and periods/events when it is not, especially for the AMOC. In the current setup, the first large AMOC anomaly peak occurs 35 years after the start of the simulations. As advective processes are also contributing (e.g. northward salt flux at 45°N), further investigation of the time scales needed to reconstruct the AMOC would require starting the nudging later, i.e. 5, 10 or 15 years before this first peak and using ensembles to further assess the robustness of reconstructing individual events. Note nevertheless that the reconstruction of the AMOC was not found to improve with the amount of time spent nudging.

This study has shown that restoring to surface temperature and salinity is able to reconstruct large regions of the deeper ocean. Fully evaluating the impact of such reconstructed initial states in hindcasts is a logical next step. The restoring strategy that works best here is the joint SST + SSS nudging everywhere, with restoring coefficients designed to provide a near zero total buoyancy forcing from the nudging itself. It allows SST nudging everywhere, in particular at high latitudes, without triggering the spurious convection events that occur close to sea-ice borders with SST only nudging. It also ensures that the right water masses are formed at the right surface density, the subsequent circulation and subduction further transporting them at depth.

Experience from ocean-only simulation shows that these dynamical features are strongly wind driven (Madec 2013, personal communication). Whereas SST nudging is able to drive the atmospheric circulation in the tropics, another step in the restoring procedure would be to drive the surface wind at mid-to-high latitudes, either forcing with the target wind stress or nudging the dynamics of the atmosphere model. Besides the dynamical forcing, this would also better drive the heat flux towards that of the target. As surface winds are better observed than sea surface salinity, the potential for subsurface reconstruction in historical frameworks may be higher than that of SSS nudging. Another perspective to connect this perfect model study to a "real world" application is to explore the impact of observational errors on the reconstruction skill of the nudging. This could be investigated by adding white noise to the SST and SSS of the target before nudging.

The detrending procedure used here filtered low frequency signals and provided time series with enough degrees of freedom to estimate significant correlation coefficients. However, such detrended time series show variance that can be quite small compared with the original variance of the un-detrended time series. This means that the correlations at depth can arise from very weak temperature and salinity variations that may not be relevant for

decadal predictability. Extending the nudging protocol to deeper layers of the ocean could help explore this issue and fully assess the performance of surface nudging only.

The perfect unforced model framework used here allows to focus on the internal variability (i.e. the goal of initialisation) and to overcome the data limitation and model biases issues. Understanding the processes at work in the models is clearly a prerequisite to using the models to understand the real world. Beyond this important step, the relevance of the present results to real world cases needs to be further explored. Ray et al. (2014, submitted) find similar overall results in historical conditions using SST-only nudging. The conclusions of this work underline the potential key role of SSS for decadal prediction and further make the case for sustained large-scale observations of this field (e.g. via SMOS and AQUARIUS). The exploration of the key role of SSS nudging in an historical setup will be reported in a subsequent study.

Acknowledgments We acknowledge Gurvan Madec and Sulagna Ray for helpful discussions, Marie-Alice Foujols and Sébastien Denvil for help with the model and data handling. This study was partly funded by the EPIDOM project (GICC) by the EU project SPECS funded by the European Commission's Seventh Framework Research Programme under the grant agreement 243964. Computations were carried out at the CCRT supercomputing centre.

Appendix: Statistical methods

The influence of the nudging method is assessed by quantifying the agreement in terms of temporal variations between the target and the nudged simulations with the help of statistical skill scores.

The first score is the correlation coefficient R (Eq. (1), significance estimated with a Student t test) to quantify the temporal agreement between the target and the nudged simulations.

$$R = \frac{1}{T-1}\frac{\sum_{t=1}^{T}((X(t)-\bar{X})(Y(t)-\bar{Y}))}{\sigma_X \sigma_Y}$$

X and Y are the same variable, X is the nudged simulation and Y the target; t represents the time, T is the length of the period, the overbar denotes a time average over which this quantity is computed (usually the length of the nudged simulations) and σ_X and σ_Y are the standard deviation of X and Y respectively. The Pearson correlation coefficient (commonly used correlation coefficient) is used for Gaussian variables, like temperature, salinity and AMOC index. For non-Gaussian variables (precipitation and mixed-layer depth), a Spearman's rank correlation coefficient is used.

To compare the amplitude of the simulated variability with the target, a Fisher F test on the ratio of variance is performed (Von Storch and Zwiers (2002)). For non-Gaussian variables (such as precipitation), the Fisher F-test is applied on the logarithm of the strictly positive values of the time series.

Estimating the significance of a correlation on 150 years of an oceanic variable as a function of depth has to deal with a low number of degrees of freedom of the time series, due to the presence of potentially dominating low frequency (multi-decadal and more). An iterative detrending procedure (see Boer (2004)) has therefore been used to remove this low frequency: a linear trend is first removed from the time series at the first iteration, and the amount of the total variance of the detrended time series that this trend represents is evaluated. If it represents more than 5 % of the variance of the detrended time series, a spline of growing order (second, third…) is iteratively removed until the variance of the lastly removed trend represents less than 5 % of the variance of the detrended time series. With this procedure, the highest order of spline removed was six. We computed the autocorrelation function of a set of randomly chosen detrended time series, and checked that this detrending procedure retains the decadal variability. It is important to note here that this detrending procedure allows estimating correlation coefficients on time series with more than ten degrees of freedom, which is much more relevant in terms of statistics than on time series presenting important trends and having not more than five degrees of freedom. However, the decadal variability of a temperature time series at more than one thousand meters in depth can be quite small compared to the amplitude of the trends. This limitation has been kept in mind when interpreting the results.

The statistical significance is computed by taking into account the serial correlation of the time series in the estimation of the number of degrees of freedom (Bretherton et al. 1999). Nevertheless, and despite the detrending procedure, some significant correlations between the free run and the target still appear. Because no causal relationship behind these correlations is assumed, we have highlighted the correlation coefficients between the nudged simulations and the target that are not significantly different (test of the difference of correlation based on the Fisher transform at the 99 % level) in absolute value from the corresponding correlation coefficient in absolute value between the target and the free run. Correlation coefficients failing this last test have to be interpreted carefully.

A bootstrap method using the 1,000 years of the control simulation was also used to estimate the significance of the correlation and gave the same estimation of significance than the method described above.

In this study, a variable or a phenomenon is qualified as "reconstructed" or "reproduced" when a certain level of agreement between a given nudged simulation and the

target, and as computed with these statistical tools, has been shown.

References

Aumont O, Bopp L (2006) Globalizing results from ocean in situ iron fertilization studies. Global Biogeochem Cycles 20(2):1–15. doi:10.1029/2005GB002591

Barnier B, Siefridt L, Marchesiello P (1995) Thermal forcing for a global ocean circulation model using a three-year climatology of ECMWF analyses. J Mar Syst 6(4):363–380. doi:10.1016/0924-7963(94)00034-9

Boer GJ (2004) Long time-scale potential predictability in an ensemble of coupled climate models. Clim Dyn 23(1):29–44. doi:10.1007/s00382-004-0419-8

Bretherton C, Widmann M, Dymnikov V, Wallace J, Bladé I (1999) The effective number of spatial degrees of freedom of a time-varying field. J Clim 12(1969):1990–2009

Collins M, Sinha B (2003) Predictability of decadal variations in the thermohaline circulation and climate. Geophys Res Lett 30(6):3–6. doi:10.1029/2002GL016504

Cox P, Stephenson D (2007) Climate change. A changing climate for prediction. Science 317(5835):207–208. doi:10.1126/science.1145956

Doblas-Reyes FJ, Andreu-Borillo I, Chikamoto Y, Garcia-Serrano J, Guemas V, Kimoto M, Mochizuki T, van Rodrigues LRL, Oldenborgh GJ (2013) Initialized near-term regional climate change prediction. Nat Commun 4:1715. doi:10.1038/ncomms2704

Du H, Doblas-Reyes FJ, García-Serrano J, Guemas V, Soufflet Y, Wouters B (2012) Sensitivity of decadal predictions to the initial atmospheric and oceanic perturbations. Clim Dyn. doi:10.1007/s00382-011-1285-9

Dufresne J-L, Foujols M-A, Denvil S, Caubel A, Marti O, Aumont O, Benshila R (2013) Climate change projections using the IPSL-CM5 earth system model: from CMIP3 to CMIP5. Clim Dyn 2123–2165. doi:10.1007/s00382-012-1636-1

Dunstone NJ, Smith DM (2010) Impact of atmosphere and sub-surface ocean data on decadal climate prediction. Geophys Res Lett 37(2):1–5. doi:10.1029/2009GL041609

Escudier R, Mignot J, Swingedouw D (2013) A 20-year coupled ocean-sea ice-atmosphere variability mode in the North Atlantic in an AOGCM. Clim Dyn. doi:10.1007/s00382-012-1402-4

Fichefet T, Maqueda MAM (1997) Sensitivity of a global sea ice model to the treatment of ice thermodynamics and dynamics. J Geophys Res 102(C6):12609. doi:10.1029/97JC00480

Frankignoul C, Kestenare E (2002) The surface heat flux feedback. Part I: estimates from observations in the Atlantic and the North Pacific. Clim Dyn 19(8):633–647. doi:10.1007/s00382-002-0252-x

Goelzer H, Mignot J, Levermann A, Rahmstorf S (2006) Tropical versus high latitude freshwater influence on the Atlantic circulation. Clim Dyn 27(7–8):715–725

Griffies SM, Biastoch A, Böning C, Bryan F, Danabasoglu G, Chassignet EP, England MH, Gerdes R, Haak H, Wallberg RW, Hazeleger W, Jungclaus J, Large WG, Madec G, Pirani A, Samuels BL, Scheinert M, Gupta AS, Severijns CA, Simmons HL, Treguier AM, Winton M, Yeager S, Yin J (2009) Coordinated ocean-ice reference experiments (COREs). Ocean Model 26(1–2):1–46

Haney RL (1971) A numerical study of the large scale response of an ocean circulation to surface heat and momentum flux. Ph.D. Dissertation, Department of Meteorology, University of California, Los Angeles

Hawkins E, Sutton R (2009) The potential to narrow uncertainty in regional climate predictions. Bull Am Meteorol Soc 90(8):1095–1107. doi:10.1175/2009BAMS2607.1

Hourdin F, Foujols M-A, Codron F, Guemas V, Dufresne J-L, Bony S, Bopp L (2013) Impact of the LMDZ atmospheric grid configuration on the climate and sensitivity of the IPSL-CM5A coupled model. Clim Dyn 40(9–10):2167–2192. doi:10.1007/s00382-012-1411-3

Joly M, Voldoire A, Douville H, Terray P, Royer JF (2007) African monsoon teleconnections with tropical SSTs in a set of IPCC4 coupled models. Clim Dyn 1–32. doi:10.1007/s00382-006-0215-8

Keenlyside N, Latif M, Botzet M (2005) A coupled method for initializing El Nino Southern Oscillation forecasts using sea surface temperature. Tellus A 340–356. doi:10.1111/j.1600-0870.2005.00107.x

Keenlyside NS, Latif M, Jungclaus J, Kornblueh L, Roeckner E (2008) Advancing decadal-scale climate prediction in the North Atlantic sector. Nature 453(7191):84–88. doi:10.1038/nature06921

Kim HM, Webster PJ, Curry JA (2012) Evaluation of short term climate change prediction in multi-model CMIP5 decadal hindcasts. Geophys Res Lett 39(10):L10701

Krinner G, Viovy N, de Noblet-Ducoudré N, Ogée J, Polcher J, Friedlingstein P, Prentice C (2005) A dynamic global vegetation model for studies of the coupled atmosphere-biosphere system. Global Biogeochem Cycles 19(1). doi:10.1029/2003GB002199

Kröger J, Müller WA, von Storch J-S (2012) Impact of different ocean reanalyses on decadal climate prediction. Clim Dyn 795–810. doi:10.1007/s00382-012-1310-7

Latif M, Collins M, Pohlmann H, Keenlyside N (2006) A review of predictability studies of Atlantic sector climate on decadal time scales. J Clim 19(23):5971–5987

Laurian A, Lazar A, Reverdin G, Rodgers K, Terray P (2006) Poleward propagation of spiciness anomalies in the North Atlantic Ocean. Geophys Res Lett 33(13):1–5. doi:10.1029/2006GL026155

Luo J–J, Masson S, Behera S, Shingu S, Yamagata T (2005) Seasonal climate predictability in a coupled OAGCM using a different approach for. J Clim 18:4474–4497. doi:10.1175/JCLI3526.1

Madec G; NEMO team (2008) NEMO ocean engine. Institut Pierre-Simon Laplace (IPSL)

Merryfield WJ, Lee WS, Boer GJ, Kharin VV, Pal B, Scinocca JF, Flato GM (2010) The first coupled historical forecasting project (CHFP1). Atmosphere-ocean 48(4):263–283

Mignot J, Frankignoul C (2003) On the interannual variability of surface salinity in the Atlantic (May 2002). 555–565. doi:10.1007/s00382-002-0294-0

Mignot Juliette, Frankignoul C (2009) Local and remote impacts of a tropical Atlantic salinity anomaly. Clim Dyn 35(7–8):1133–1147. doi:10.1007/s00382-009-0621-9

Msadek R, Dixon KW, Delworth TL, Hurlin W (2010) Assessing the predictability of the Atlantic meridional overturning circulation and associated fingerprints. Geophys Res Lett 37(19):1–5. doi:10.1029/2010GL044517

Persechino A, Mignot J, Swingedouw D, Labetoulle S, Guilyardi E (2013) Decadal predictability of the Atlantic meridional overturning circulation and climate in the IPSL-CM5A-LR model. Clim Dyn. doi:10.1007/s00382-012-1466-1

Pohlmann H, Jungclaus J, Köhl A, Stammer D, Marotzke J (2009) Initializing decadal climate predictions with the GECCO oceanic synthesis: effects on the North Atlantic. J Clim 22(14):3926–3938. doi:10.1175/2009JCLI2535.1

Schneider N, Venzke S, Miller A, Pierce DW, Deser C, Barnett TP, Latif M (1999) Pacific thermocline bridge revisited. Geophys Res Lett 26(9):1329–1332

Smith DM, Cusack S, Colman AW, Folland CK, Harris GR, Murphy JM (2007) Improved surface temperature prediction for the coming decade from a global climate model. Science 317(5839):796–799. doi:10.1126/science.1139540

Speer K, Tziperman E (1992) Rates of water mass formation in the North Atlantic. J Phys Oceanogr 22:93–104

Speer BK, Guilyardi E, Madec G, Cnrs POI (2000) Southern Ocean transformation in a coupled model with and without eddy mass fluxes. Tellus A 52(5):554–565

Stepanov VN, Haines K, Smith GC (2012) Assimilation of RAPID array observations into an Ocean model. Quart J R Meteorol Soc 138(669):2105–2117. doi:10.1002/qj.1945

Swingedouw D, Braconnot P, Delecluse P, Guilyardi E, Marti O (2007a) The impact of global freshwater forcing on the thermohaline circulation: adjustment of North Atlantic convection sites in a CGCM. Clim Dyn 28:291–305

Swingedouw D, Braconnot P, Delecluse P, Guilyardi E, Marti O (2007b) Quantifying the AMOC feedbacks during a 2xCO2 stabilization experiment with land-ice melting. Clim Dyn 29:521–534

Swingedouw D, Mignot J, Labetoulle S, Guilyardi E, Madec G (2013) Initialisation and predictability of the AMOC over the last 50 years in a climate model. Clim Dyn 40:2381–2399. doi:10.1007/s00382-012-1516-8

Taylor KE, Stouffer RJ, Meehl GA (2012) An overview of CMIP5 and the experiment design. Bull Am Meteoroll Soc 93(4):485–498

Valcke S (2012) The OASIS3 coupler: a European climate modelling community software. Geosci Model Dev Discuss 5(3):2139–2178. doi:10.5194/gmdd-5-2139-2012

Von Storch H, Zwiers FW (2002) Statistical analysis in climate research. Cambridge University Press, p 496

Walin G (1982) On the relation between sea-surface heat flow and thermal circulation in the ocean. Tellus 34(2):187–195. doi:10.1111/j.2153-3490.1982.tb01806.x

Xie S-P, Carton JA (2004) Tropical Atlantic variability: patterns, mechanisms, and impacts. Geophys Monogr Ser 147:121–142. doi:10.1029/147GM07

Yu L (2011) A global relationship between the ocean water cycle and near-surface salinity. J Geophys Res 116(C10):C10025. doi:10.1029/2010JC006937

Zhang R, Delworth TL (2006) Impact of Atlantic multidecadal oscillations on India/Sahel rainfall and Atlantic hurricanes. Geophys Res Lett 33(17):L17712. doi:10.1029/2006GL026267

Zhang S, Harrison MJ, Rosati A, Wittenberg A (2007) System design and evaluation of coupled ensemble data assimilation for global oceanic climate studies. Mon Wea Rev 135(10):3541–3564. doi:10.1175/MWR3466.1

Zhang S, Rosati A, Delworth T (2010) The adequacy of observing systems in monitoring the atlantic meridional overturning circulation and North Atlantic climate. J Clim 23(19):5311–5324. doi:10.1175/2010JCLI3677.1

Zhang R, Zheng F, Zhu J, Pei Y (2012) Modulation of El Nino-Southern Oscillation by Freshwater Flux by Freshwater Flux and Salinity Variability in the Tropical Pacific. Adv Atmos 29(4):647–660. doi:10.1007/s00376-012-1235-4.1

Zheng F, Zhang R-H (2012) Effects of interannual salinity variability and freshwater flux forcing on the development of the 2007/08 La Niña event diagnosed from Argo and satellite data. Dyn Atmos Oceans 57:45–57. doi:10.1016/j.dynatmoce.2012.06.002